LUND UNIVERSITY

Soft X-ray spectroscopy of liquids: Development and characterization of a flat jet nozzle system with experimental applications

Gallo, Tamires

2024

Soft X-ray spectroscopy of liquids:
Development and characterization of a flat jet nozzle system with experimental applications

TAMIRES GALLO
DEPARTMENT OF PHYSICS | FACULTY OF SCIENCE | LUND UNIVERSITY

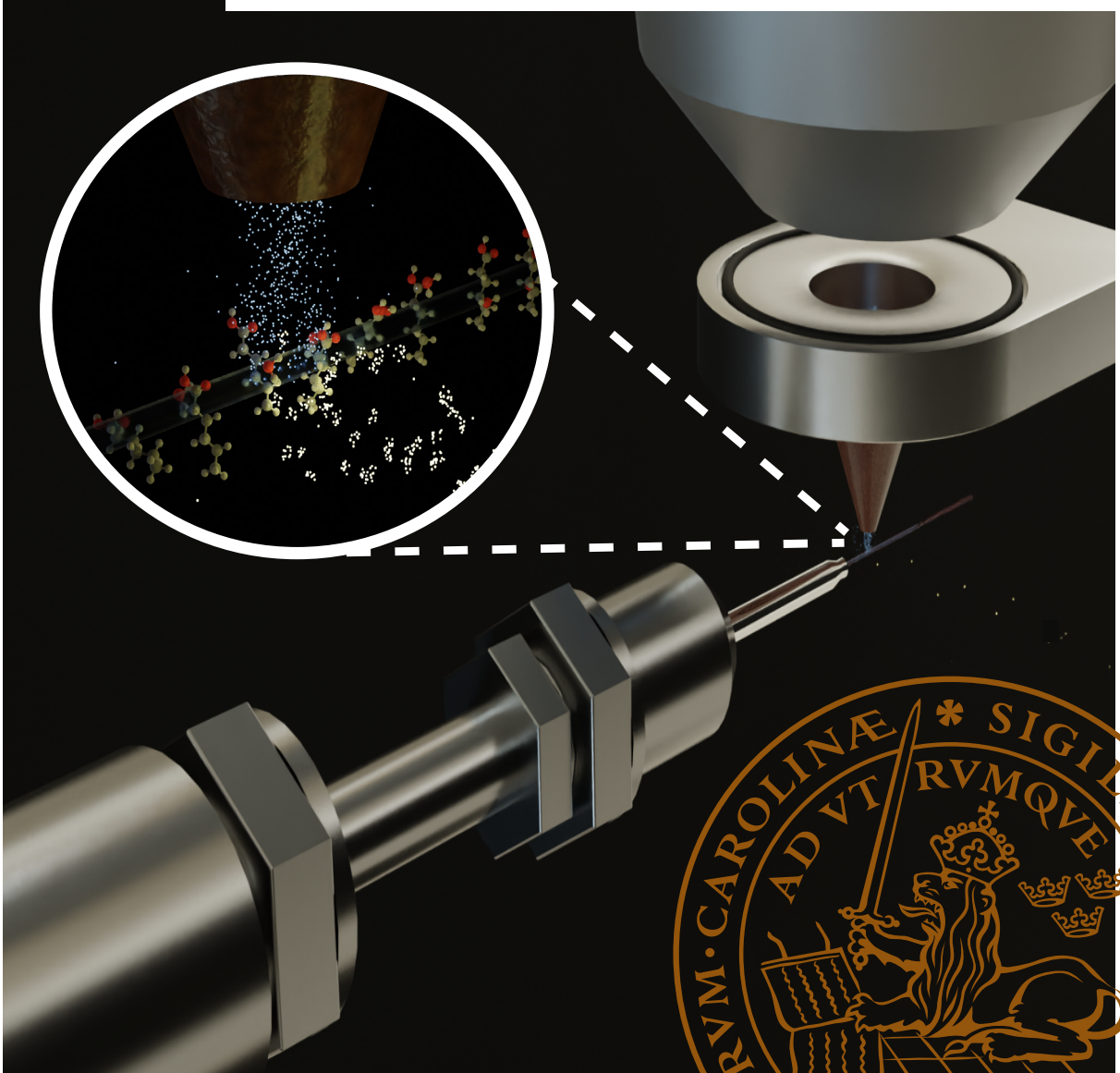

Soft X-ray spectroscopy of liquids: Development and characterization of a flat jet nozzle system with experimental applications

Soft X-ray spectroscopy of liquids: Development and characterization of a flat jet nozzle system with experimental applications

by Tamires Gallo

LUND
UNIVERSITY

Thesis for the degree of Doctor of Philosophy
Thesis advisors: Dr. Gunnar Öhrwall, Dr. Noelle Walsh, Dr. Joana Valerio, Dr. Jan Knudsen, Prof. Joachim Schnadt
Faculty opponent: Håkan Rensmo

To be presented, with the permission of Faculty of Science of Lund University, for public criticism in the Rydberg Lecture Hall at Department of Physics on Thursday 24 October 2024 2024 at 13:15.

Organization
LUND UNIVERSITY

Department of Physics
Box 188
SE–221 00 LUND
Sweden

Author(s)
Tamires Gallo

Document name
DOCTORAL DISSERTATION

Date of disputation
2024-10-24

Sponsoring organization

Title and subtitle: Soft X-ray spectroscopy of liquids: Development and characterization of a flat jet nozzle system with experimental applications.

Abstract

In this thesis, I report the development and implementation of 3D-printed flat sheet nozzles for advancing liquid-phase soft X-ray spectroscopy at MAX IV Laboratory in Paper II. The nozzles presented here, discussed in Paper III, were custom designed for the FlexPES beamline and deliver flat liquid sheets of micrometer thickness. The planar shape of the liquid leaf gen-erated with these nozzles serves to significantly simplify the measurement geometry, allowing a more accurate interpretation of experimental results. In addition, I also demonstrate, that these significantly thinner sheets facilitate transmission-mode X-ray absorption measurements, thus expanding experimental capabilities for liquid jet users at MAX IV.

To demonstrate the type of experiments that could benefit from the use of flat sheet nozzles, we studied the impact of angular distribution on X-ray photoelectron spectroscopy (XPS) data from aqueous solutions. The study comprises two parts: In paper I, the angular distribution of N 1s photoelectrons from an aqueous ammonium nitrate solution was investigated using a cylindrical microjet and the surface propensity of the solute ions in the same sample was investigated using a liquid flat jet. In paper IV, we investigated the angular effects observed in photoelectron spectra recorded for a range of potassium carboxylate aqueous solutions. In particular, we explored how molecular orientation, influenced by alkyl chain length, affects the observed X-ray photoelectron spectra.

Key words
Liquid microjet, liquid flat jet nozzle, Soft X-ray spectroscopy

Classification system and/or index terms (if any)

Supplementary bibliographical information

Language
English

ISSN and key title

ISBN
978-91-8104-203-0 (print)
978-91-8104-204-7 (pdf)

Recipient's notes

Number of pages
114

Price

Security classification

Signature _____ Date 2024-09-10

Soft X-ray spectroscopy of liquids: Development and characterization of a flat jet nozzle system with experimental applications

by Tamires Gallo

LUND
UNIVERSITY

Cover illustration front: Picture showing my research.

Cover illustration back: Photograph of a water flat jet produced by a 3D-printed nozzle under atmospheric conditions (Paper III).

Funding information: Carl Trygger Foundation for the development of the flat-jet setup at FlexPES (grant CTS 20:502). Aeryleanska resestipendiefonden (94501). Bokelunds resestipendiefond (94507).

Faculty of Science, Department of Physics

ISBN: 978-91-8104-203-0 (print)
ISBN: 978-91-8104-204-7 (pdf)
ISSN: <ISSN number>

Printed in Sweden by Media-Tryck, Lund University, Lund 2024

Media-Tryck is a Nordic Swan Ecolabel certified provider of printed material. Read more about our environmental work at www.mediatryck.lu.se

Printed matter 3041 0903

MADE IN SWEDEN

Dedicated to Ana Liz and Vicente,
who brought light into my life, and inspired me to keep going

Contents

List of publications ii
Abstract vii
Acknowledgements viii
Popular summary in English xii
Populärvetenskaplig sammanfattning på svenska xiii
Resumo científico popular em Português xiv
1 Introduction 1
2 Concepts and Methods 6
2.1 Properties of liquids and solutions 6
2.2 X-ray spectroscopy 11
2.3 X-ray Absorption Spectroscopy (XAS) 13
2.4 X-ray Photoelectron Spectroscopy (XPS) 13
2.5 Comparison between XAS and XPS 13
2.6 Liquid jet research from the renaissance to synchrotron applications 14
2.7 Simulation of electron spectra 16
3 Electron spectroscopies 17
3.1 Photoionization processes 17
3.2 Photoelectron Angular Distributions (PAD) 18
3.3 X-ray Absorption Spectroscopy (XAS) 22
4 Experimental methods 24
4.1 Light sources for X-ray spectroscopy 24
4.2 FlexPES beamline 28
4.3 Liquid jets for spectroscopy measurements 33
5 Results and Experimental Outcomes 42
5.1 Nozzle designs for liquid flat jet 42
5.2 3D-print nozzles at EuXFEL 43
5.3 Commissioning flat jet nozzles 48
5.4 MAX IV infrastructure for implementing 3D flat jet nozzles . . 54
5.5 Application of the flat-jet in real scientific cases 56
6 Summary of papers and outlook 59
7 References 63

Appendix: Details about the MAX IV 3D jet infrastructure **75**

List of publications

This thesis is based on the following publications, referred to by their Roman numerals:

I **Aqueous Ammonium Nitrate Investigated Using Photoelectron Spectroscopy of Cylindrical and Flat Liquid Jets**
T. Gallo, G. Michailoudi, J. Valerio, L. Adriano, M. Heymann, J. Schulz, R. Marinho, F. Callefo, N. Walsh, G. Öhrwall

The Journal of Physical Chemistry B 128, 28, 6866–6875 (2024). DOI:10.1021/acs.jpcb.4c01755

I took part in the planning and performance of some of the experiments at MAX IV, performed data analysis, and took part in the preparations of the first draft of the manuscript and subsequent revision.

II **Development of a flat jet delivery system for soft X-ray spectroscopy at MAX IV.**
T. Gallo, L. Adriano, M. Heymann, A. Wrona, N. Walsh, G. Öhrwall, F. Callefo, S. Skruszewicz, M. Namboodiri, R. Marinho, J. Schulz, J. Valerio

Journal of Synchrotron Radiation 31, 1285-1292 (2024). DOI:10.1107/S1600577524006611

I was the main responsible for the project, which included initiating contact with the Sample Environment and Characterization (SEC) and Spectroscopy and Coherent Scattering (SCS) groups from EuXFEL, discussing the development of the 3D-printed nozzles, conducting stability characterization at EuXFEL. Also, I was the main responsible for the identification and procurement of the necessary equipment, I was the main responsible for the installation and commissioning of a new setup, planned and executed the commissioning experiments at MAX IV, analyzed the data, and prepared the first draft of the manuscript, as well as participating in subsequent revisions.

III **Optimization of Flat Sheet Nozzles for Soft X-ray Spectroscopy.**

T. Gallo, J. Valerio, L. Adriano, M. Heymann, A. Wrona, N. Walsh, G. Öhrwall, F. Callefo, S. Skruszewicz, M. Namboodiri, R. Marinho, J. Schulz
Manuscript

I was the main responsible for the project, discussing the development of the 3D-printed nozzles, conducting stability characterization at EuXFEL, analyzing the data, and preparing the first draft of the manuscript, as well as participating in subsequent revisions.

IV **Photoelectron angular distributions from aqueous potassium carboxylate salts**
T. Gallo, G. Michailoudi, K. Toledo, R. Marinho, O. Björneholm, N. Walsh, G. Öhrwall

Manuscript

I took part in the planning and performance of some of the experiments at MAX IV, performed the data analysis, and took part in the preparations of the first draft of the manuscript and subsequent revision.

The following publications are not included in this thesis where the order of authorship on each individual paper accurately reflects my level of contribution to the respective projects.

V **Application of synchrotron Analytical techniques in Archeology.**

D. Galante, F. Rodrigues, L. Maldanis, **T. Gallo**
Journal of the Laboratory of Education and Research in Anthropology and Archaeology (Lepaarq), 15(30), 277-289. Nov. 2018.
DOI:10.15210/lepaarq.v15i30.13522

VI **Li-self doping effect on the LiAl5O8 luminescent properties.**

V. Teixeira, A. Silva, I. Manali, **T. Gallo**, D. Galante, N. Ferreira, A. Andrade, M.Rezende
Optical Materials, 94, 160-165. May. 2019.
DOI:10.1016/j.optmat.2019.05.029

VII **Luminescent properties of Li(Ga1-xCrx)5O8 (LGCO) phosphors.**

V. Teixeira, I. Manali, **T. Gallo**, D. Galante, D. Barbosa, C. Paschoal, R. Silva, M. Rezende
Ceramics International,46(10), 15779-15785. March. 2020.
DOI:10.1016/j.ceramint.2020.03.122

VIII **Atomic Layer Deposition of Hafnium Oxide on InAs: Insight from Time-Resolved in *Situ* Studies.**

G. D'Acunto, A. Troian, E. Kokkonen, F. Rehman, Y. Liu, S. Yngman, Z. Yong, S. McKibbin, **T. Gallo**, E. Lind, J. Schnadt, R. Timm
ACS Applied Electronic Materials, 2(12), 3915-3922. Nov. 2020.
DOI:10.1021/acsaelm.0c00775

IX **HIPPIE: a new platform for ambient-pressure X-ray photoelectron spectroscopy at the MAX IV Laboratory.**

S. Zhu, M. Scardamaglia, J. Kundsen, R. Sankari, H. Tarawneh, R. Temperton, L. Pickworth, F. Cavalca, C. Wang, H. Tissot, J. Weissenrieder, B. Hagman, J. Gustafson, S. Kaya, F. Lindgren, I. Källquist, J. Maibach, M. Hahlin, V. Boix, **T. Gallo**, F. Rehman, G. D'Acunto, J. Schnadta, A. Shavorskiya
Journal of Synchrotron Radiation, 28(2), 624-636. March. 2021.
DOI:10.1107/S160057752100103X

X **Area-selective Electron-beam Induced Deposition of Amorphous-BNx on Graphene.**

V. Boix, C. Struzzi, **T. Gallo**, N. Johansson, G. D'Acunto, Z.Yong, A. Zakharov, Z. Li, J. Schnadta, A. Mikkelsen, J. Knudsen
Applied Surface Science, 557, 149806. April. 2021.
DOI:10.1016/j.apsusc.2021.149806

XI **Stroboscopic operando spectroscopy of the dynamics in heterogeneous catalysis by event-averaging.**

J. Knudsen, **T. Gallo**, V. Boix, M. Strømsheim, G. D'Acunto, C. Goodwin, H. Wallander, S. Zhu, M. Soldemo, P. Lömker, F. Cavalca, M. Scardamaglia, D. Degerman, A. Nilsson, P. Amann, A. Shavorskiy, J. Schnadt
Nature Communications, 12, 6117. Oct. 2021.
DOI:10.1038/s41467-021-26372-y

XII **The Cobalt Oxidation State in Preferential CO Oxidation on CoOx/Pt(111) investigated by Operando X-ray Photoemission Spectroscopy.**

E. Rattigan, Z. Sun, **T. Gallo**, M. Nino, S. Parreiras, C. Martín-Fuentes, J. Martin-Romano, D. Écija, C. Escudero, I. Villar, J. Rodríguez-Fernández, J. Lauritsen
Physical Chemistry Chemical Physics, 24, 9236-9246. April. 2022.
DOI:10.1039/D2CP00399F

XIII **Following the Kinetics of Undercover Catalysis with APXPS and the Role of Hydrogen as an Intercalation Promoter.**

V. Boix, M. Scardamaglia, **T. Gallo**, G. D'Acunto, M. Strømsheim, F. Cavalca, S. Zhu, A. Shavorskiy, J. Schnadt, J. Knudsen
ACS Catalysis, 12(16), July. 2022.
DOI: 10.1021/acscatal.2c00803

XIV **Graphene as an Adsorption Template for Studying Double Bond Activation in Catalysis.**

V. Boix, W. Xu, G. D'Acunto, J. Stubbe, **T. Gallo**, M. Strømsheim, S. Zhu, M. Scardamaglia, A. Shavorskiy, K. Reuter, M. Andersen, J. Knudsen
The Journal of Physical Chemistry C, 126(33), 14116–14124. Aug. 2022.
DOI:10.1021/acs.jpcc.2c02293

XV **Protective effects of halite to vacuum and VUV: A potential scenario during a young sun superflare.**

X. Abrevaya, D. Galante, P. Tribelli, O. Oppezzo, F. Nobrega, G. Araujo, F. Rodrigues, P. Odert, M. Leitzinger, M. Ricardi, E. Varela, **T. Gallo**, J. Sanz-Focada, I. Ribas, F. Mello, F. Rodler, M. Cerini, A. Hanslmeier, J. Horvath
Astrobiology (Cover article), 23(3), 245-268. Mar. 2023.
DOI:10.1089/ast.2022.0016

Abstract

In this thesis, I report the development and implementation of 3D-printed flat sheet nozzles for advancing liquid-phase soft X-ray spectroscopy at MAX IV Laboratory in Paper II. The nozzles presented here, discussed in Paper III, were custom designed for the FlexPES beamline and deliver flat liquid sheets of micrometer thickness. The planar shape of the liquid leaf generated with these nozzles serves to significantly simplify the measurement geometry, allowing a more accurate interpretation of experimental results. In addition, I also demonstrate, that these significantly thinner sheets facilitate transmission-mode X-ray absorption measurements, thus expanding experimental capabilities for liquid jet users at MAX IV.

To demonstrate the type of experiments that could benefit from the use of flat sheet nozzles, we studied the impact of angular distribution on X-ray photoelectron spectroscopy (XPS) data from aqueous solutions. The study comprises two parts: In paper I, the angular distribution of N 1s photoelectrons from an aqueous ammonium nitrate solution was investigated using a cylindrical microjet and the surface propensity of the solute ions in the same sample was investigated using a liquid flat jet. In paper IV, we investigated the angular effects observed in photoelectron spectra recorded for a range of potassium carboxylate aqueous solutions. In particular, we explored how molecular orientation, influenced by alkyl chain length, affects the observed X-ray photoelectron spectra.

Acknowledgements

Completing a PhD is a challenge in itself, and my journey was filled with both obstacles and intense storms that made me change my course. I'm grateful to have survived and to have had everyone involved. This journey was far from easy, with a new project halfway through, a pandemic, and an accident that resulted in a concussion, taking almost a year to recover (please, everyone, wear a helmet! Haha). I am now stronger and happy to have had great people by my side who were my foundation throughout this journey.

First, I would like to thank Jan Knudsen and Joachim Schnadt (Achim) for accepting me as a PhD student and for all the knowledge I gained from both of you at the beginning of my journey. Jan, thank you for teaching me my first steps in the world of spectroscopy, writing, and inspiring me to create professional figures. Achim, thank you for all your support and the insightful discussions from which I learned a lot.

I would also like to thank Gunnar Öhrwall and Noelle Walsh for accepting me as a student under unexpected conditions and guiding me through the second half of my journey. Gunnar, I gained a lot of knowledge from you; you are exceptional not only for your expertise in instrumentation and spectroscopy but also for your kindness and problem-solving approach, which has been an inspiration to me. Noelle, thank you for all your efforts to keep everything on track, your reviews (doing your "magic" with words), our coffees, and your trust in my work. Thank you both for giving me the freedom and trust to handle our project; this was invaluable.

Joana Valerio and Joachim Schulz, thank you so much for guiding me in the world of 3D printing and nozzles, for your supervision, trust, and time, and for opening the doors of EuXFEL to me. Joachim, you have been like a co-supervisor to me, always guiding me brilliantly. Thank you for welcoming me warmly into your labs and for accepting the idea of this project from the very beginning! Joana, thank you for everything! You not only taught me about nozzles and 3D printing but also reignited my passion for being in the lab. Through our collaboration, I gained not only a co-supervisor but also a friend.

Michael Heymann (Micha), thank you for being my first contact in the 3D printing world, for introducing me to the sample environment group at EuXFEL, and for your patience in explaining how everything works. Luigi Adriano and Agnieszka Wrona (Aga), I cannot thank you enough for all your time and effort in teaching me in the labs. Our lunches, coffees, and great moments will stay with me for life! Both of you guided me in my first physical contact with the

nozzles, and I appreciate your openness in sharing your knowledge. A special thanks to Luigi for all the discussions about nozzle designs, instrumentation, and everything else. I learned a lot from you! Thank you! I would also like to extend my gratitude to the Sample Environment and Characterization (SEC) and Spectroscopy and Coherent Scattering (SCS) groups at EuXFEL for their invaluable support and collaboration. Your collective expertise and assistance have been crucial in advancing this research.

I would also like to thank Ann Kull; the "writing days" you organized were not only great moments to focus on writing but also a source of strength during one of the most challenging times in my life. You showed me the path, and I would never have been able to finish this thesis without you. Matilda Eklund and Louise Burfield, thank you for your beautiful work; it was life-changing. You gave me strength and helped me breathe! Malin Rantzer and Lars Åke, thank you for being by my side and helping me navigate through the storm. Rainer Timn, thank you for your support and guidance during difficult changes in my PhD journey. Edvin Lundgren and Patrik Wirgin, thank you for bringing light and happiness to the department. You are the rock that supports many of us (students)! Margit Andersson, Maxim Tchaplyguine, and Sverker Werin, you have brought joy and laughter into my life during lunch and coffee breaks. Your stories, wisdom, and shared memories of old times have been a delightful source of happiness and inspiration throughout my journey.

Ricardo Marinho, thank you for your unwavering support and guidance throughout my PhD journey. Your insightful advice during our long night shifts, along with the many laughs we shared, was invaluable. Your time in Sweden made a significant impact on my journey! A special thanks to Joao Bassos for your assistance during my recovery from a concussion when I couldn't look at screens. Your expertise in CAD was essential in developing the catcher concept presented in this thesis.

Pascale Deen, Rasmus Toft-Petersen, Liam Whitelegg, and the Spectroscopy Team, I would like to extend my sincere thanks for your incredible support and flexibility, which have been crucial in helping me complete this journey. Pascale, your encouragement and understanding as I balanced work at ESS and writing this thesis have been vital. Thank you!

I would like to express my deepest gratitude to Silvana. Your unwavering support and guidance have been instrumental in helping me navigate the challenges of my PhD journey. Without your expertise, compassion, and encouragement, I would not have been able to persevere and reach this milestone. Your dedication to my well-being has made all the difference, and for that, I'm eternally grateful.

I would also like to thank my second family in Sweden (alphabetical order) Artur, Caiafa, Caissa, Cassia, Carla, Clarissa, Felipe, Fernando, Henrique, Juliano, Kalle, Karina, Kim, Kliu, Lorrayne, Marco, Margareta, Matheus, Mirko, Natalia, Tomas, Umi, Vanessa, and Weronica. Your friendship has been a cornerstone of my journey. Your kindness and unwavering support have been a constant source of comfort, with encouragement and positivity have been a driving force. Also, all laughter and joy all of you have brought light to my darkest days, and your wisdom and advice have been invaluable. Your encouragement and belief in my abilities have inspired me to keep pushing forward, even when the path seemed insurmountable. I am profoundly thankful for your support and for being an integral part of my journey. Having all of you made this journey so much more enjoyable.

Nestor, who brought me (alphabetical order) Esther (Rudy), Joakim and Natalia (Bonnie and Drake), Magesh (Kayal), and Ximena (Lily). Thank you for being with me during the happy and not-so-happy moments. All your support, encouragement, kindness, empathy and generosity have made a significant impact. Your positivity and friendship have been invaluable. Thank you all for being there for me, through the highs and lows.

I would like to express my deepest gratitude to Doug, my previous supervisor and dear friend. Your unwavering support and guidance have been invaluable throughout this journey. Your insightful feedback, patience, and encouragement have significantly shaped my research and personal growth. I am deeply thankful for the countless hours you dedicated to mentoring me, and for always being there to provide wisdom and reassurance during the toughest moments.

A heartfelt thank you to Adriano, Flavia, and Veronica. Your constant presence and encouragement during the most challenging moments made this PhD journey much lighter and more manageable. Flavia, your keen insights and thoughtful advice have been a source of great inspiration. Adriano, your technical expertise and willingness to help at any time have been crucial to my progress. Veronica, your emotional support and positivity have been a beacon of light, keeping me motivated and focused. I am truly grateful for your friendship and unwavering support.

I would like to extend my deepest appreciation to my friends from the CH for life, who were a precious gift from the pandemic (alphabetical order): Alceu, Aline, Ana (and George), Andrezinho, Cassio, Carla, JC, Lina, Maria, Marnie, Matheus, Michelli, Mike, Monia, Paulinha, Pablo Kassio, PX, Rapha, Roberta, Val, and Wany. Despite the challenges we faced, the pandemic had a silver lining—it brought us together. Our deep connection and friendship have been

incredibly important throughout this journey. Your kind words, shared moments of joy, and unwavering support have been a constant source of strength. You have been there to listen to my cries of both happiness and sadness, always lifting me up and helping me see the brighter side of things. I am truly grateful for your companionship and the joy you have brought into my life. Each of you has contributed uniquely to my journey, whether through late-night conversations, shared laughter, or simply being a comforting presence. Thank you all for being such an integral part of my life and for making this journey not only bearable but truly enjoyable. I am forever grateful for each one of you.

I would like to thank Skupina Allan Kardec group for being an integral part of my life. Your unwavering support and companionship through all critical moments and experiences have been invaluable. You have shown me how to navigate through life's storms without losing focus, kindness, and happiness. The presence of all of you has been a beacon of light, guiding me with wisdom and compassion. Thank you for sharing this journey with me and for being a source of strength and inspiration.

Finally, to my beloved family; my mother (mae), Douglas, Fernanda, Vó Luiza, Vó Therezinha, Thabata, and the children Ana Liz, Vicente, Matheus, Jhonny, Jack, and Lyria. Your unwavering love and support have been my anchor throughout this journey. Mae, your strength and encouragement have been my guiding light. Douglas and Fernanda, your belief in me kept me going. Vó Luiza and Vó Therezinha, your wisdom and warmth have been a source of comfort. Thabata, your cheerfulness, and positivity have brightened my days. And to the little ones, Ana Liz, Vicente, Lyria, Matheus, Jhonny, and Jack, your smiles and laughter have been a constant reminder of the joy in life. Thank you all for being my rock and my inspiration.

Popular summary in English

Have you ever wondered how scientists peer into the hidden structures of molecules? In short, X-ray spectroscopy of liquid jets is a cutting-edge technique that allows us to unravel the mysteries of matter on a molecular scale. In this thesis, I will dive into the world of liquid jets, synchrotron radiation, and 3D-printed nozzles, while demystifying the science behind it.

Liquid jet spectroscopy is like a cosmic spotlight that illuminates the tiniest actors on the molecular stage. Imagine shooting a thin stream of liquid (our "jet") into the path of powerful synchrotron radiation, a type of light generated by accelerating charged particles. As synchrotron light interacts with the liquid, it reveals crucial information about the molecules within.

Why Liquid Jets?

1. Flat vs. Curved: Geometry matters! Unlike traditional cylindrical jets, which curve as they flow, flat liquid jets provide a clean canvas surface for analysis. Think of it as comparing a bumpy road with a smooth runway: the flat jet wins every time.

2. Angular Insights: By tweaking the angle at which we measure the synchrotron radiation, we gain insights into electron behavior. Papers I and IV in our thesis showcase this beautifully, revealing how measurement geometry influences electron spectroscopy data.

In collaboration with EuXFEL, 3D-printed nozzles have been developed for our flat-jet system. These tiny marvels provide a precise and controlled flow of liquid. Imagine a miniature fountain pen, but instead of ink, it delivers molecules for analysis.

Liquid jet spectroscopy helps us to understand surface properties, such as how ammonium nitrate behaves close to a liquid surface. This knowledge has implications for everything from catalysis to drug delivery. Our flat jet system found its home on the FlexPES beamline. But the possibilities extend beyond—other MAX IV beamlines could benefit from liquid jets in the future.

Next time you sip your morning coffee, remember that liquid jets are not just for caffeine addicts: they are unlocking the secrets of the universe, one molecule at a time. Liquid jet spectroscopy is our backstage pass to the molecular theater, where electrons pirouette and atoms waltz. So raise your glass to science and let the liquid jets flow!

Populärvetenskaplig sammanfattning på svenska

Har du någonsin undrat hur forskare tittar in i molekylers dolda strukturer? Kort sagt är Röntgenspektroskopi på vätskestrålar en banbrytande teknik som låter oss reda ut materiens mysterier på molekylär nivå. I denna avhandling kommer jag att dyka in i världen av vätskestrålar, synkrotronstrålning och 3D-printade munstycken, samtidigt som jag avdramatiserar vetenskapen bakom det.

Vätskestråle-spektroskopi är som en kosmisk strålkastare som belyser de minsta aktörerna på den molekylära scenen. Föreställ dig att spruta en tunn stråle av vätska (vår ”jet”) in i vägen för kraftfull synkrotronstrålning, en typ av ljus som genereras genom att accelerera laddade partiklar. När synkrotronljuset interagerar med vätskan avslöjar det avgörande information om molekylerna inuti.

Varför vätskestrålar?

1. Flat vs. krökt: Geometrin spelar roll! Till skillnad från traditionella cylindriska strålar, som har en krökt yta, ger flata vätskestrålar en plan och ren dukyta för analys. Tänk på det som att jämföra en gropig väg med en slät landningsbana: den flata strålen vinner varje gång.

2. Vinklade insikter: Genom att ändra vinkeln relativt synkrotronstrålningen i vilken vi mäter får vi insikter om elektronbeteende. Artikel I och IV i vår avhandling visar detta vackert och avslöjar hur mätgeometrin påverkar elektronspektroskopisk data.

I samarbete med EuXFEL har 3D-printade munstycken utvecklats för vårt flatstrålesystem. Dessa små underverk ger ett precist och kontrollerat flöde av vätska. Föreställ dig en miniatyrreservoarpenna, men istället för bläck levererar den molekyler för analys. Vätskestråle-spektroskopi hjälper oss att förstå ytegenskaper, som hur ammoniumnitrat beter sig. Denna kunskap har konsekvenser för allt från katalys till läkemedelsleverans. Vårt flatstrålesystem fann sitt hem på strålröret FlexPES. Men möjligheterna sträcker sig bortom det - andra MAX IV-strållinjer skulle kunna dra nytta av vätskestrålar i framtiden. Nästa gång du sippar på ditt morgonkaffe, kom ihåg att vätskestrålar inte bara är för koffeinmissbrukare: de låser upp universums hemligheter, en molekyl i taget. Vätskestråle-spektroskopi är vårt backstage-pass till den molekylära teatern, där elektroner gör piruetter och atomer valsar. Så höj ditt glas för vetenskapen och låt vätskestrålarna flöda!

Resumo científico popular em Português

Você já se perguntou como os cientistas investigam as estruturas ocultas das moléculas? Em resumo, a espectroscopia de jato líquido é uma técnica de ponta que nos permite desvendar os mistérios da matéria em escala molecular. Nesta tese, mergulharei no mundo dos jatos líquidos, radiação síncrotron e "agulhas" impressos em 3D, enquanto desmistifico a ciência por trás disso. A espectroscopia de jato líquido é como um holofote cósmico que ilumina os menores atores no palco molecular. Imagine disparar um fino jato de líquido (nosso "jato") no caminho de uma poderosa radiação síncrotron, um tipo de luz gerada pela aceleração de partículas carregadas. À medida que a luz síncrotron interage com o líquido, ela revela informações cruciais sobre as moléculas dentro dele.

Por que Jatos Líquidos?

1. Plano vs. Curvo: A geometria importa! Ao contrário dos jatos cilíndricos tradicionais, que se curvam à medida que fluem, os jatos líquidos planos fornecem uma superfície limpa para análise. Pense nisso como comparar uma estrada esburacada com uma pista lisa: o jato plano vence sempre.

2. Perspectiva Angular: Ajustando o ângulo em que medimos a radiação síncrotron, obtemos insights sobre o comportamento dos elétrons. Os artigos I e IV dessa tese mostram isso lindamente, revelando como a geometria de medição influencia os dados de espectroscopia de elétrons.

Em colaboração com o EuXFEL, "agulhas" impressas em 3D foram desenvolvidos para o nosso sistema de jato plano. Essas pequenas maravilhas fornecem um fluxo preciso e controlado de líquido. Imagine uma caneta-tinteiro em miniatura, mas em vez de tinta, ela entrega moléculas para análise. A espectroscopia de jato líquido nos ajuda a entender propriedades de superfície, como o comportamento do nitrato de amônio. Esse conhecimento tem implicações para tudo, desde catálise até entrega de medicamentos. Nosso sistema de jato plano encontrou seu lar na linha de feixe FlexPES. Mas as possibilidades se estendem além—outras linhas de feixe do MAX IV poderiam se beneficiar dos jatos líquidos no futuro.

Da próxima vez que você tomar seu café da manhã, lembre-se de que os jatos líquidos não são apenas para viciados em cafeína: eles estão desvendando os segredos do universo, uma molécula de cada vez. A espectroscopia de jato líquido é nosso passe de bastidores para o teatro molecular, onde elétrons piruetam e átomos valsam. Então, levante seu copo para a ciência e deixe os jatos líquidos fluírem!

1 Introduction

Spectroscopy - From Newton's first experiments to cutting-edge synchrotron research

Spectroscopy, the study of the interaction between matter and electromagnetic radiation, has been a cornerstone of scientific discovery for centuries. This powerful analytical technique has revolutionized our understanding of the universe, from the smallest atoms to the most distant stars. The story of spectroscopy begins in 1666 when Sir Isaac Newton conducted his groundbreaking experiments with sunlight and prisms[1]. Newton discovered that white light could be separated into a spectrum of colors, laying the foundation for the field of spectroscopy. However, it was not until the early nineteenth century that spectroscopy truly began to take shape as a scientific discipline. In 1802, William Wollaston observed dark lines in the solar spectrum, but it was Joseph von Fraunhofer who, in 1814, systematically studied and cataloged these lines. Fraunhofer's work marked the birth of modern spectroscopy, as he demonstrated that these dark lines were characteristic of specific elements. This discovery opened up a new world of possibilities for analyzing the composition of distant stars and planets. The mid-19th century saw rapid advances in spectroscopic techniques. Gustav Kirchhoff and Robert Bunsen developed the spectroscope in 1859, which allowed for the precise measurement of spectral lines. Their work led to the discovery of new elements, including cesium and rubidium, through spectral analysis. As the understanding of atomic structure grew in the early 20th century, so did the applications of spectroscopy[2]. The development of quantum mechanics provided a theoretical framework for interpreting spectral data, leading to a deeper understanding of atomic and molecular structure.

The invention of the laser in 1960 by Theodore Maiman marked another significant milestone in spectroscopy. Laser spectroscopy allowed for unprecedented precision in measuring atomic and molecular energy levels, opening up new avenues for research in fields such as chemistry, physics, and materials science. In recent decades, the advent of synchrotron radiation sources has propelled spectroscopy to new heights.

Synchrotron-based spectroscopy

Synchrotrons, large particle accelerators that produce intense beams of light across a wide range of wavelengths, have enabled scientists to probe the atomic and electronic structure of materials with unprecedented detail and accuracy.

Synchrotron-based spectroscopy techniques, such as X-ray absorption spectroscopy (XAS) and X-ray photoelectron spectroscopy (XPS), allow researchers to study the local atomic environment, chemical bonding, and electronic properties of materials. These advanced methods have found applications in diverse fields, including materials science, environmental research, and pharmaceutical development. The use of synchrotron radiation in spectroscopy has revolutionized our ability to unveil the atomic organization of materials. Scientists can now investigate complex systems, such as catalysts, batteries, and biological molecules, with atomic-level precision. This has led to breakthroughs in areas like energy storage, drug design, and nanotechnology. From Newton's simple prism experiments to the cutting-edge synchrotron facilities of today, spectroscopy has come a long way. As technology continues to advance, spectroscopic techniques are becoming increasingly sophisticated, allowing us to probe deeper into the nature of matter and unlock the secrets of the universe around us. In recent times, surface electron spectroscopy on liquid samples has emerged as an important branch of spectroscopy that provides insight into the electronic structure of liquids as well as ion or molecule solvation at the liquid surface, allowing us to determine the behavior of a given ion or molecule at the surface compared to the bulk liquid.[3,4].

Liquid jets for X-ray spectroscopy research

One of the few ways to study liquids in vacuum is through the use of a liquid microjet. This method can introduce small enough amounts of liquids into vacuum to enable experiments that can determine key properties of the studied samples such as chemical composition, surface structure, and the distribution of solutes in the solution, molecular interaction, and bonding. In addition, liquid jets play an important role in numerous practical applications, including engineering, agriculture, fuel injection, and medicine[1,5,6].

The main experimental challenge that arises when investigating the electronic structure of liquids using soft X-ray spectroscopy techniques[1] such as photoemission spectroscopy (PES) is related to the need for high vacuum (at least 10^{-5}mbar) in the area of experimentation[6]. The incident soft X-ray radiation is absorbed by gaseous particles, and the departing electrons have a very short inelastic mean free path in a dense gas. In addition, a further complication arises from the fact that most liquids are highly volatile and either evaporate or freeze when placed in a vacuum. Despite these difficulties, Hans and Kai Siegbahn were able to perform the first successful PES experiments on liquid

[1] given the E range of soft X-rays is $\sim$ 100 to 2500/3000 eV

formamide in 1973[6–10], and during the next decade, various experimental approaches were tested, the most successful being the use of a rotating metal disc that continuously refreshed the liquid surface[10].

Significant advances in the field of liquid XPS were made in 1988 when Manfred Faubel[11] and colleagues developed a new microjet technique that proved highly suitable as a liquid sample delivery method for electron spectroscopy on volatile liquids, including water[6,12]. The method involved using a small glass nozzle with an opening diameter on the order of tens of µm (prepared using laser drilling) and forcing the liquid sample through the nozzle by applying a strong backing pressure, thus forming a tiny cylindrical beam, "liquid jet" - that is introduced into the vacuum chamber at a speed of around 100 m/s. The key to success was to make the system small enough so that the evaporation of the liquid results in a rapid drop-off in the density of gaseous molecules surrounding it. This approach improved the experimental conditions considerably, decreasing the interaction between the emitted photoelectrons and the surrounding gas and increasing the likelihood that the photoelectrons will reach the electron analyzer[11,13]. Additionally, the fast flow of the liquid jet results in continuous exposure of a new liquid surface and reduces the issue of charging during the photoemission process.

Following many years of work with traditional cylindrical jets, a production process for a gas dynamic virtual nozzle (GDVN) was developed, which involved the microfabrication of a microchannel with a narrowing constriction to increase the velocity of the liquid flow in the jet along with the use of a supersonic gas jet to focus the liquid into a thin stream[14]. Furthermore, recent advances in femtosecond laser writing using 2-photon polymerization (2PP), have allowed 3D-printing of high-resolution nozzle tips in a robust polymer material with arbitrary three-dimensional geometry[15].

Liquid microjets facilitate the analysis of the liquid-vacuum interface, which approaches the liquid-gas surface, as well as a wide range of other phenomena. For instance, XPS on liquid jets can be used to study the behavior of ions or molecules in aqueous solutions that simulate the composition of water droplets that evaporate from the oceans and participate in regulating the planet's temperature, such as those that capture atmospheric (CO_2) gas[16]. Liquid surface electron spectroscopy can also be applied to molecules of high biological interest, such as amino acids, providing a promising avenue for future research. By studying the electronic structure and behavior of amino acids (building blocks of proteins) at the liquid-air interface, researchers can gain valuable information about their interactions, conformations, and potential role in biological processes. This knowledge could contribute significantly to our understanding of fundamental

biological phenomena.[17–21]

Scientific motivation for the work in this thesis

The primary objective of this thesis is to develop an innovative setup to facilitate the use of liquid flat jets for XPS and XAS studies at the MAX IV Laboratory. This development is driven by:

Limitations of Cylindrical Liquid Jets: Traditional cylindrical liquid jets, commonly used in XPS experiments, are typically tens of micrometers thick. Given that the transmission length of soft X-rays is on the order of a few microns, these cylindrical microjets are inherently unsuitable for soft X-ray transmission spectroscopy. Additionally, the thickness of cylindrical microjets can vary significantly within the interaction volume, leading to uncertainties in XPS data analysis.

Advantages of Flat Jets: In contrast, flat jets offer a distinct advantage due to their planar surface, which facilitates the investigation of surface orientation effects. This characteristic makes flat jets particularly suitable for detailed surface studies, thereby addressing the limitations posed by cylindrical jets.

Development of Flat Jet Setup: To overcome these limitations and enable new types of measurements, **Paper II** proposed a sample introduction system featuring a flat liquid surface. This flat-liquid jet setup is specifically designed for the FlexPES photoemission endstation, providing a valuable tool for future users. In the later stages of this thesis, a flat jet solution using 3D-printed nozzles was developed in collaboration with EuXFEL, as detailed in **Paper III**. This solution, intended for the MAX IV user community, was adapted for implementation on the FlexPES beamline. Furthermore, custom nozzles of a similar design have the potential for use at other MAX IV beamlines.

Impact of angular distributions on XPS Data from Aqueous Solutions: This doctoral work also includes two papers that investigate the influence of photoelectron angular distribution on XPS data from aqueous solutions. **Paper I** and **Paper IV** used conventional cylindrical jets to examine how photoelectron angular distribution affects intensities by varying the electron emission angle, photon energy, and solute composition in aqueous solutions. **Paper I** focuses on ammonium nitrate. This is an interesting sample due to the ongoing debate in the literature about the distribution of nitrate ions near the surface of aqueous solutions, and the surface sensitivity of photoelectron spectroscopy makes it an attractive technique to study this issue. The paper provides valuable insights

into the surface behavior of ammonium nitrate, but the measurements also highlighted the limitations of cylindrical liquid jet systems due to their curved geometry. Later measurements using 3D-printed flat jet nozzles gave additional data on the depth distribution, which played a crucial role in establishing the surface properties of nitrate and ammonium. **Paper IV** presents experimental results on potassium carboxylate salts, which serve as effective model systems for studying the surface activity of solutes in aqueous solutions. These results provide insights into how different chain lengths affect surface enrichment. The results of **Paper I** and **Paper IV** clearly highlight the influence of measurement geometry on electron spectroscopy data.

2 Concepts and Methods

2.1 Properties of liquids and solutions

Liquids are essential compounds for life because they provide an environment in which chemical reactions can occur. Water covers about 70% of our planet's surface and plays an essential role in the metabolic processes of living organisms[22,23]. It is unique in its ability to act as a solvent, an electrolyte, and catalyst in chemical reactions simultaneously. This makes it an essential element for the chemical and biological reactions that occur in the human body[22,24]. Aqueous environments provide a complex environment for dissolved molecules, where solvation processes significantly influence their behavior. Solvation, the interaction between a solute and a solvent, induces a myriad of effects including structural alterations, charge redistribution, and even molecular dissociation[25]. The differential behavior of the solutes at the liquid-gas interface compared to the bulk phase further complicates this scenario[26]. A comprehensive understanding of liquid properties, especially in the interfacial regions, is essential to advance fields ranging from biology to materials science.[27,28]

The determination of the physical and structural properties of liquid is a challenging task, especially in understanding its surface properties at the molecular level. The gas phase, for example, is characterized by atoms or molecules that interact very weakly with each other, allowing them to move independently. In contrast, the solid phase is characterized by strong interactions between particles (molecules and atoms), which force them to move only at the sites of their crystalline lattice in the case of crystalline solids. Liquids exhibit properties that are common to both of these phases. In the liquid phase, the energy of interaction between particles is comparable to that of the thermal energy, and their dynamics resemble those of the gas phase, while their density is similar to that of the solid state. With a negligible loss of precision, one could consider the liquid phase as a hybrid between the solid and gas phases. For liquids that do not have strong directional interactions between their molecules (non-associated liquids), liquid nitrogen is easier to describe, because of its lack of directional interactions. In other words, their molecules do not form hydrogen bonds or other types of strong interactions that would cause them to have a more defined local structure. Associated liquids, such as water, have a more defined local structure due to hydrogen bonding between molecules[29,30].

The physical properties of liquids that are particularly relevant for this work include surface tension, molecular orientation at liquid surfaces, and liquid viscosity.

Surface tension refers to the force acting on the surface of a liquid that minimizes its surface area. This property results from the intermolecular forces between particles in the liquid. At the surface of the liquid, molecules experience an unbalanced force that pulls them towards the interior of the liquid, leading to cohesive forces. However, the molecules in the bulk of the liquid experience equal forces on all sides. Surface tension plays a critical role in various phenomena, such as capillary action, wetting, and bubble formation.

The viscosity of the liquid measures the resistance of the liquid to flow, and it is determined by the internal friction that arises due to the interactions between the molecules in the liquid. Lastly, molecular orientation at liquid surfaces arises due to intermolecular forces at the surface. These forces e.g. cause molecules to orient themselves with their long axis perpendicular to the surface. This property is particularly relevant in the study of surface chemistry, where the orientation of molecules can affect chemical reactions and surface reactivity[31].

With the current stage of development of liquid surface electron spectroscopy, it is possible to examine how the phenomenon of ion or molecule solvation occurs on the liquid surface and whether there is any difference in the behavior of a given ion or molecule on the surface compared to the bulk liquid.

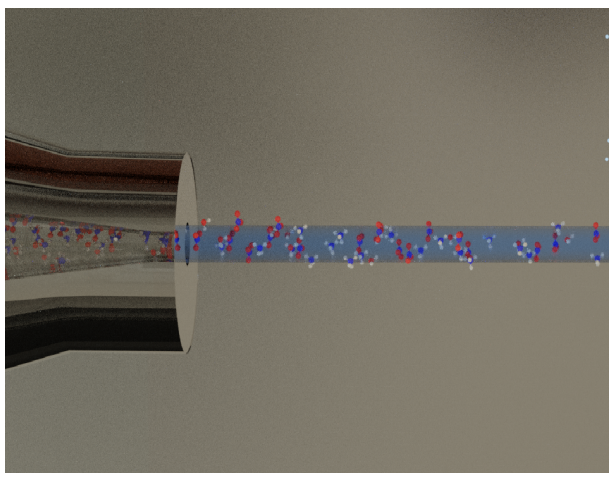

Figure 1: Schematic representation of a liquid jet environment, with NH_4^+ and NO_3^- ions in water. Atoms are in red Oxygen, gray Hydrogen, and blue Nitrogen.

Basic properties of water

The water molecule has a bent molecular geometry, with an angle of about $104.5°$ [32,33] between the hydrogen-oxygen-hydrogen atoms. In a simple picture this geometry can be understood as being due to that the 8 valence electrons (6 from O, 2 from H) form four orbitals, and to minimize repulsion these orbitals are arranged in an approximately tetrahedral configuration, resulting in the bent structure. The oxygen atom in water is more electronegative than the hydrogen atoms, leading to a polar covalent bond, with a partial negative charge on the oxygen and a partial positive charge on the hydrogens. This polar nature of water molecules leads to hydrogen bonding, a strong intermolecular force. In liquid water, hydrogen bonding occurs when the hydrogen atoms of a water molecule are attracted to the oxygen atom of a neighboring water molecule, due to the partial negative charge on the oxygen atom and the partial positive charge on the hydrogen atoms. Each water molecule can form up to four hydrogen bonds: two through its hydrogen atoms and two through its lone pair electrons.

Latimer and Rodebush first suggested that a free pair of electrons on one water molecule could exert enough force on the hydrogen held by a pair of electrons on another water molecule to bind the two molecules together, according to Lewis theory [34–36].

The molecular geometry and charge distribution of water lead to several important properties:

- **High Cohesion and Surface Tension:** Due to hydrogen bonding, water molecules are strongly attracted to each other, resulting in high cohesion and surface tension.
- **High Specific Heat Capacity:** Water can absorb a lot of heat without a significant change in temperature, which is crucial for regulating Earth's climate.
- **Density Anomaly:** Water is most dense at 4°C, and its solid form (ice) is less dense than its liquid form, allowing ice to float.

The hydrogen bond between two water molecules is asymmetric, with one molecule acting as a donor and the other acting as an acceptor. Each water molecule can accept and donate two hydrogen bonds in a near-tetrahedral arrangement. Another interesting aspect of hydrogen bonds is that it facilitate the transport of H_3O^+ and OH^- ions [29,35,37], and in fact, electron spectroscopy of liquid jets have contributed to the understanding of this phenomenon [38].

Furthermore, the polar nature of water leads to a larger dipole moment per molecule for polar solutes compared to that of the isolated form, because the water molecules can align themselves with the partial charges of the solute molecules, enhancing their polarity. This makes water a polar solvent that can dissolve polar solutes more easily than nonpolar solutes, following the rule of 'like dissolves like'.

Ammonium nitrate

Ammonium nitrate is a chemical compound that is commonly found in fertilizers and is composed of nitrogen, hydrogen, and oxygen. It is acidic in nature since it is derived from a weak base (NH_3) and a strong acid (HNO_3). When ammonium nitrate is added to water, the polar water molecules interfere with the ionic bonds that hold the compound together, causing the ions to disperse.

The dissociation of ammonium nitrate (into ($NH_4{}^+$) and ($NO_3{}^-$)) in water is an endothermic reaction that absorbs energy from the environment and makes the solution cold. On the other hand, the compound itself can at elevated temperatures decompose spontaneously, into water, nitrous oxide, or nitrogen and oxygen molecules, in a highly exothermic reaction. These properties make ammonium nitrate useful in various industrial applications, including as an explosive and as a component in cold packs[39].

Surface propensity refers to the tendency of a substance to accumulate at the surface of a liquid. This phenomenon is due to the difference in intermolecular forces between the molecules on the surface and those on the bulk of the liquid. For example, surfactants are molecules that have hydrophobic (water-repelling) and hydrophilic (water-attracting) regions. When added to water, surfactants tend to accumulate on the surface of water as a result of their hydrophobic regions.

The surface propensity of a solvated ion can be influenced by various factors, including temperature, pH, concentration, and the presence of other ions or compounds[40–42]. At the surface of an aqueous ammonium nitrate solution, the ammonium and nitrate ions can exhibit different behaviors, resulting in changes in surface tension, film thickness, and other surface properties. Understanding the surface propensity of ammonium nitrate in aqueous solutions could thus potentially help in various applications, such as controlling foam formation in industrial processes or designing efficient fertilizers.

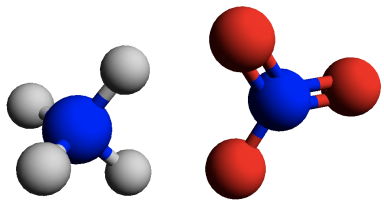

Figure 2: NH_4 and NO_3 ions representation, atoms are in red Oxygen, gray Hydrogen, and blue Nitrogen.

Potassium carboxylate salts

Carboxylate salts are ionic compounds that consist of a metal cation and a carboxylate anion. The carboxylate anion has the general formula $RCOO^-$, where R is an organic group. The carboxylate group is formed by the deprotonation of a carboxylic acid group, which has the general formula RCOOH. Carboxylic acids can have one or more carboxyl groups in their structure.

In this thesis, we have studied aqueous solutions of potassium carboxylate salts, including formate, acetate, propionate, butyrate, and hexanoate. The structure of the molecules is presented in Figure 3, where some applications for these chemicals are given in the caption. For the larger molecules (propionate, butyrate, and hexanoate), the salt solutions were prepared by reacting the corresponding acids (propionic, butyric, and hexanoic acid) with potassium hydroxide in aqueous solution, whereas for the smaller ones (formate and acetate), the compounds were obtained commercially.

In general, carboxylate salts exhibit a wide range of chemical properties in aqueous solutions that are dependent on their size, structure, and pH of the solution. These properties make them important in various applications, such as catalysts, electrolytes, and reagents in organic synthesis.

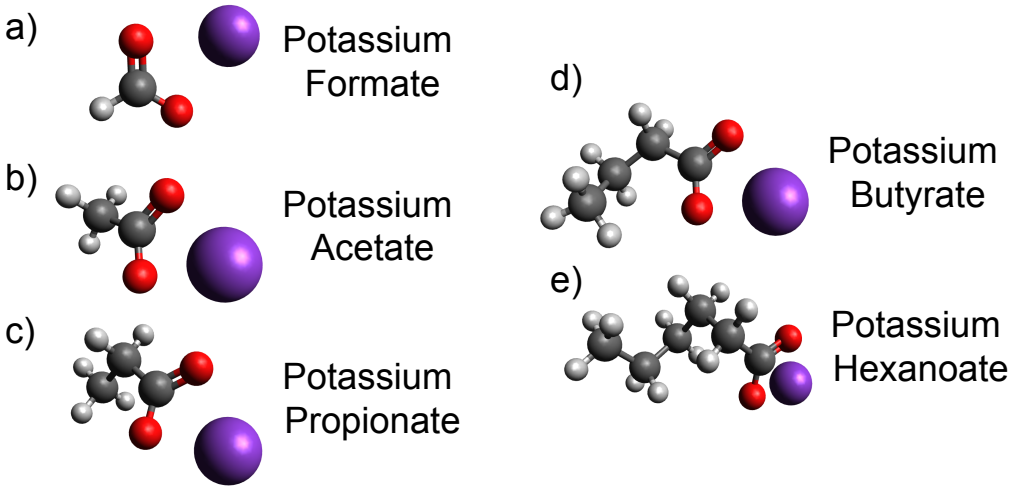

Figure 3: (a) Potassium formate is used in oil and gas drilling and as a de-icer agent for roads, runways, and other surfaces.(b) Potassium acetate is used as a food additive, flavor enhancer, pH control agent, and firming agent, and in medicine for respiratory stimulation and dialysis solutions. (c) Potassium propionate is a food preservative to inhibit mold and bacteria growth in various food products. (d) Potassium butyrate has several health benefits, including supporting the growth of beneficial gut bacteria, improving gut barrier function, and reducing inflammation. In the field of medicine, it has been used as a therapeutic agent for the treatment of various diseases and conditions. (e) Potassium hexanoate is found in some foods and has potential uses as a treatment, flavor, and fragrance ingredient, but its safety as a food additive is uncertain.

2.2 X-ray spectroscopy

The term "Spectroscopy" comes from the Latin word "*spectrum*" meaning "appearance" or "image" and the Greek word "*skopein*" meaning "to see", which means to observe or examine. Spectroscopy is a scientific technique that includes studying how matter interacts with electromagnetic radiation and involves measuring and analyzing the spectrum of radiation that is absorbed, emitted, or scattered by a sample. It is a powerful tool that can be used to investigate the chemistry of liquid surfaces. Using various spectroscopic techniques, it is possible to monitor changes in the electronic structure of molecules as they undergo chemical reactions.

One important type of radiation used for spectroscopy is X-rays, which Wilhelm Conrad Röntgen discovered in 1895 and for which he was later awarded the Nobel Prize in physics in 1901. X-ray spectroscopy can be used to investigate the core levels of atoms, which is relevant in many fields of natural science, as well as in medicine and materials science. One of the most versatile and widely used sources of X-rays is the synchrotron radiation facility (4.1), which uses high-energy electrons to produce intense, highly focused beams of X-rays.

In the energy range of interest for the work in this thesis, photon-electron interactions can be described by two main mechanisms: photoemission and photoabsorption, as shown in Figure 4.

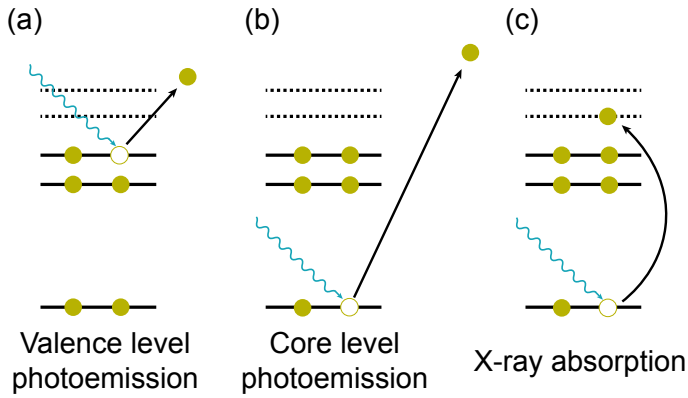

Figure 4: Schematic representation of some fundamental mechanisms of interaction between X-rays and matter. (a) In valence band spectroscopy, an electron from the valence band, or the highest occupied molecular orbital in the case of molecules, is excited into the vacuum. (b) A similar phenomenon takes place during core-level photoemission, with the distinction that the ejected electron originates from a core level. (c) In X-ray absorption, an electron from the core levels is excited into an unoccupied orbital.

Photoemission or photoelectron spectroscopy is a technique used to study the chemical composition of sample surfaces on the basis of the theory of photoelectric effect. The phenomenon was first observed by A. E. Becquerel in 1839 and confirmed in 1887 by Heinrich Hertz. However, it was only in 1905 that Einstein provided a satisfactory explanation of the phenomenon, which resulted in him being awarded the Nobel Prize in physics in 1921. In 1981, Kai Siegbahn was awarded the Nobel Prize in physics for developing Electron Spectroscopy for Chemical Analysis (ESCA). ESCA, or XPS, involves irradiating the sample with X-rays and measuring the kinetic energy of the emitted photoelectrons. By analyzing the energy distribution of the photoelectrons, it is possible to identify the chemical species present at the surface.

In addition to XPS, other spectroscopic techniques can also be used to probe the chemistry of liquid surfaces. For example, in XAS, by measuring the energy and intensity of the transmitted X-rays, information can be obtained about the electronic structure and chemical environment of the atoms in the sample. In the case of liquid surfaces, by using a surface sensitive detection technique such as electron yield, XAS can provide valuable insights into the behavior of molecules and ions at the interface between the liquid and the surrounding atmosphere or substrate.

In general, XAS and XPS are complementary techniques used to study the electronic structure of materials. Below the basic framework for XAS and XPS in the soft X-ray regime is outlined.

2.3 X-ray Absorption Spectroscopy (XAS)

XAS measures the absorption of X-rays as a function of energy, providing information about the local electronic and geometric structure of materials. The absorption coefficient, $\mu(E)$, is a key parameter and is described by the Beer-Lambert law[2].

$$I(E) = I_0\, e^{-\mu(E)t} \tag{1}$$

where I_0 is the incident intensity, $I(E)$ is the transmitted intensity and t is the thickness of the material. Frequently, transmission XAS experiments are difficult to perform, and then other measures of the photon absorption are used instead of the transmitted radiation, such as electron or photon yield.

2.4 X-ray Photoelectron Spectroscopy (XPS)

XPS is based on the photoelectric effect and measures the kinetic energy of electrons ejected from a material. The binding energy, E_{binding}, is calculated using:

$$E_{\text{binding}} = h\nu - E_{\text{kinetic}} - \phi \tag{2}$$

where $h\nu$ is the energy of the incident X-ray photon, E_{kinetic} is the kinetic energy of the ejected electron measured by the spectrometer, and ϕ is the work function of the spectrometer.

2.5 Comparison between XAS and XPS

- **Information Provided:** XAS provides information about the local electronic and geometric structure, whereas XPS gives insights into the elemental composition and chemical states.
- **Probed property:** XAS probes unoccupied electronic states, while XPS probes occupied states.

- **Depth Sensitivity:** XPS is usually surface-sensitive due to the limited escape depth of photoelectrons. In contrast, XAS typically probes deeper into the material, but this depens on the detection mode. For example, partial electron yield with kinetic energies of a few hundred eV (Auger yield) can be surface-sensitive.

Both XPS and XAS are versatile tools for studying the chemistry of liquid surfaces and can provide valuable insight into the mechanisms of chemical reactions and the behavior of molecules at interfaces. In general, spectroscopic techniques offer quantitative and highly sensitive means of monitoring chemical reactions at the liquid surface.

The energy range for soft X-ray spectroscopies is between $\sim$ 100eV to a few keV[43,44]. Since soft X-rays are strongly absorbed by air, experiments using photons in this energy range can only take place under vacuum conditions.

In the case of electron-based spectroscopies, the electrons emitted from the irradiated sample have a very short inelastic mean free path when traversing a dense gas (order of a micrometer at atmospheric pressures), making it difficult for them to reach the detector. This problem is even more pronounced when measuring on liquid samples, as most liquids are volatile and will evaporate or freeze quickly in a vacuum. The introduction of a liquid into a vacuum environment, is quite technically challenging and techniques such as liquid microjets, droplet beams, and flow cells are employed to maintain a clean and controlled sample environment.

2.6 Liquid jet research from the renaissance to synchrotron applications

The history of liquid jet research dates back to the 15^{th} century when Leonardo da Vinci and Mariotte debated the reasons for the drop of water from an orifice. Da Vinci proposed that it was due to gravity, while Mariotte suggested that it was due to cohesive forces[45,46]. In the 19^{th} century, Savart conducted the first experimental examination of liquid jets and the instabilities along their surface[47]. Plateau then discovered that surface tension was the root cause of these instabilities[45]. In 1931, Weber added the viscosity factor to the stability analysis of liquid jets from the Rayleigh analysis[48].

For soft X-ray XAS the most direct way of recording an absorption spectrum is by using "transmission" mode. However, cylindrical jets typically have a thicknesses of 6-50 micrometers and are too thick compared to the typical attenuation

lengths of soft X-rays in liquids. The sample thickness must therefore be limited, typically in the submicrometer to a few micrometer range[49]. In addition, the optical path length in the liquid is not homogeneous, and the (macroscopic) curvature of the surface makes studies of surface orientation effects more difficult. Recently, several methods have been described to achieve flat jets of ≈µm thickness in a vacuum, which potentially could be used for photoelectron and absorption spectroscopy[50].

To achieve a flat jet, the crucial part is the nozzle design. The development of flat-sheet jets of sub-micrometer thickness, high stability, and optical flatness has enabled several novel achievements in science. For example, Knoska et al.[51] highlight that the development of flat-sheet jets has been crucial in advancing XFEL technology, allowing for high-resolution imaging of biological molecules and complex materials at atomic scales. Similarly, Fondell et al.[52] demonstrate that time-resolved photoelectron spectroscopy has benefited from flat jets by enabling the study of ultrafast electron dynamics in liquids and at interfaces, providing insights into chemical reactions and energy transfer processes. Additionally, improved precision in surface-sensitive techniques like XPS and near-edge X-ray absorption fine structure (NEXAFS) spectroscopy has been achieved, thanks to the stability and reproducibility of flat jets[53]. The development of flat-sheet jets has thus facilitated significant advancements in various scientific fields[54,55].

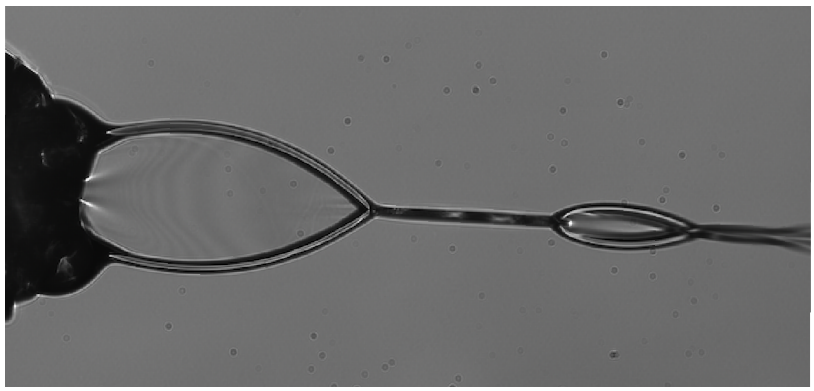

Figure 5: Water flat jet image produced by a 3D-printed nozzle at atmospheric condition.

Liquid flat sheets can be produced by obliquely colliding two identical laminar jets[50], using a planar chip[53], or 3D-printed models as presented in this thesis, see figure 5 (and chapters 4.3 and 5). A converging 3D-printed nozzle can use He gas, which causes the liquid to expand and form a sheet in the shape of a leaf with a thicker rim. A fluid chain consisting of multiple sheets can be created, each subsequent link decreasing in size until it eventually merges into a single jet.

2.7 Simulation of electron spectra

Simulations of electron spectra are useful for interpreting experimental XPS data with the aim of improving the accuracy of quantitative analysis. Analysis can be performed using a variety of methods, including Monte Carlo simulations, which is employed in the software used in **Paper I** if this work - the SESSA package (Simulation of Electron Spectra for Surface Analysis). SESSA, developed by the National Institute of Standards and Technology (NIST)[56], performs simulations with the aim to give a quantitative interpretation of electron spectra for a given sample composition.

SESSA employs Monte Carlo simulations to model the transport of electrons through materials. This involves tracking the paths of many electrons as they undergo random scattering events, both elastic and inelastic, to predict the resulting spectra. To achieve this, the program relies on databases of photoionization cross sections, inelastic mean free paths (IMFPs), and elastic scattering cross sections. SESSA allows users to define complex sample geometries and compositions, simulating how these affect the XP (X-ray photoelectron) spectra. The software can simulate spectra for samples with multiple layers or nanostructures, taking into account the different scattering and attenuation properties of each layer or component. It uses mathematical models to predict how the intensity of photoelectron peaks varies with depth and composition. For depth profiling, the software calculates the attenuation of photoelectron signals as a function of depth, using the effective attenuation length (EAL), which combines the effects of IMFP and elastic scattering. By incorporating these mathematical models and computational techniques, SESSA provides a robust framework for simulating XP spectra, enabling detailed quantitative analysis of surface compositions and structures. This makes it an invaluable tool for researchers working in surface science and materials analysis.

3 Electron spectroscopies

This thesis focuses on photon-electron interaction in the soft X-ray range, which involves two main processes: core-level photoemission and photoabsorption. When the photon energy exceeds the ionization potential, a core electron may be emitted, and this is referred to as X-ray photoemission or photoelectron spectroscopy (XPS). When monochromatic radiation is used, these emitted electrons will exhibit well-defined energy spectra. By studying photoemission spectra, we gain insight into electronic structures, chemical states, and material properties, contributing significantly to fields like surface physics, material science, and nanotechnology.

Photoabsorption occurs when matter absorbs a photon, transferring its energy to an electron. Below a core-level threshold, absorption can lead to a transition to an empty level, which yields information about the unoccupied electronic structure. This may also serve as an initial step to observe decay processes in atoms or molecules. X-ray absorption spectroscopy (XAS) involves scanning the photon energy across a specific energy range (around a core edge) and measuring the photoabsorption cross section.

3.1 Photoionization processes

Einstein proposed that an atom can be ionized when irradiated by high-energy photons, and an electron is removed – a photoelectron. This phenomenon is known as the photoelectric effect. The kinetic energy (E_{kinetic}) of the photoelectron can be measured and the corresponding binding energy (E_{binding}) is determined if the incident photon energy ($h\nu$) is known. The binding energy is the identity of the specific element in the sample and will vary depending on its chemical surroundings. As already shown above, it can be described from the following equation,

$$E_{\text{binding}} = h\nu - E_{\text{kinetic}} - \phi \tag{3}$$

where h is Planck's constant, ν is the frequency of the incident light, and ϕ is the work function. A simple analysis can determine the elemental composition of a sample, and a more complex analysis requires a detailed understanding of surface chemistry, especially when there are many possible surface species.

Because of the short mean free path of electrons in condensed matter, XPS is a surface-sensitive technique that allows the determination of the chemical

composition of a material. In XPS, a sample is bombarded with X-rays, causing photoemission of core electrons.

For XPS analysis, the photoelectrons are collected in the hemispherical electron analyzer using an electrostatic lens that focuses the emitted electrons onto the entrance slit of the analyzer, as illustrated in Figure 6. The analyzer consists of two concentric hemispherical electrodes, and it disperses the electrons in energy and focuses them from the entrance slit onto the detector. The kinetic energies of the emitted electrons can be measured by the analyzer, and the number of electrons collected is plotted against this energy. The binding energy, calculated from the known photon energy, is element-specific and is used to determine the composition of the material. For solid samples, the sample and analyzer are in electrical contact, aligning their Fermi levels, and this is used as the energy reference of the binding energy scale. For liquid and gas samples, where there is no electric contact, the energy scale is instead usually referenced to the vacuum level, the lowest energy at which the electron is free from the sample. In practice, for liquids we normally measure the kinetic energy with respect to some reference level, often the O 1s core level or the $1b_1$ valence level of water in the case of aqueous solutions, to estimate the binding energy. More accurate estimates of the binding energy of liquids can be done by applying a bias voltage the sample and measuring the kinetic energy above the cut-off, representing the zero kinetic energy point[57].

After outer valence ionization, often only relatively long-lived radiative decay transitions are possible. If a core electron is expelled, the system becomes unstable. The core hole may decay by being filled with a valence or a higher-lying core-level electron, releasing excess energy as a photon (normal X-ray emission) or initiating an autoionization event (normal Auger decay), schematically shown in Figure 7. The system may end up in highly charged states if further relaxation is possible.

3.2 Photoelectron Angular Distributions (PAD)

PADs refer to the angular distribution of photoelectrons that are emitted from a sample when it is subjected to photon excitation. In a simple picture, the process can be considered in terms of conservation of angular momentum: The total angular momentum of the sample and the photon before the photoionization event must be the same as that for the ion and the photoelectron after. For example, in the case of photoionization of an s orbital in a free atom, since the angular momentum is unchanged in the atom by the removal of the electron, the unit of angular momentum of the photon must be transferred to the photo-

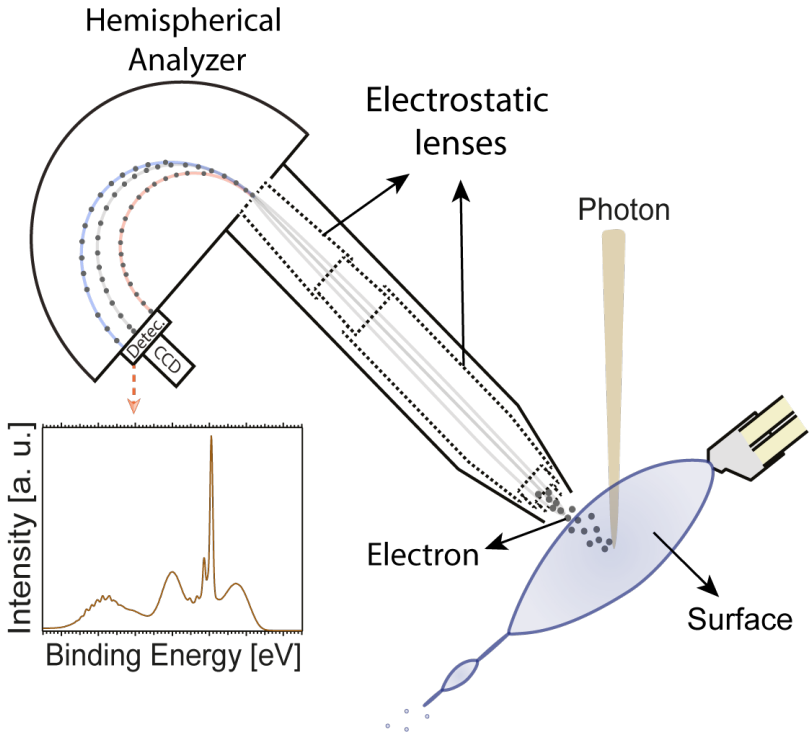

Figure 6: Schematic of XPS experimental setup where a sample is exposed to X-rays, resulting in the emission of electrons. These photoelectrons are then directed into a hemispherical electron analyzer equipped with an electrostatic lens. The analyzer focuses the emitted electrons onto a detector. The collected electrons' kinetic energies are measured, and the number of electrons detected can be plotted against their binding energy or kinetic energy. This binding energy, which is element-specific, aids in determining the material's composition.

electron, which therefore is emitted as a p wave, with the angular distribution of the p orbital. In more complex systems, where scattering and other mechanisms that could affect the angular momentum, such as rotations, occur, the description becomes much more involved. The PADs can still provide information about the electronic structure of the sample, including its bond angles, orbital symmetries, and other geometric arrangements.

The differential cross section for photoelectron emission is analogous to other scattering processes, such as Rayleigh or Compton scattering, where the angular distribution provides critical information about the interaction dynamics. However, in the case of photoelectron emission, the focus is on the electronic structure and the symmetry of the atomic or molecular orbitals involved. For linearly polarized radiation it is given by[58]

$$\frac{\mathrm{d}\sigma}{\mathrm{d}\Omega} = \frac{\sigma}{4\pi}\left(1 + \frac{\beta}{2}\left(3\,\cos^2\theta - 1\right)\right) \,, \tag{4}$$

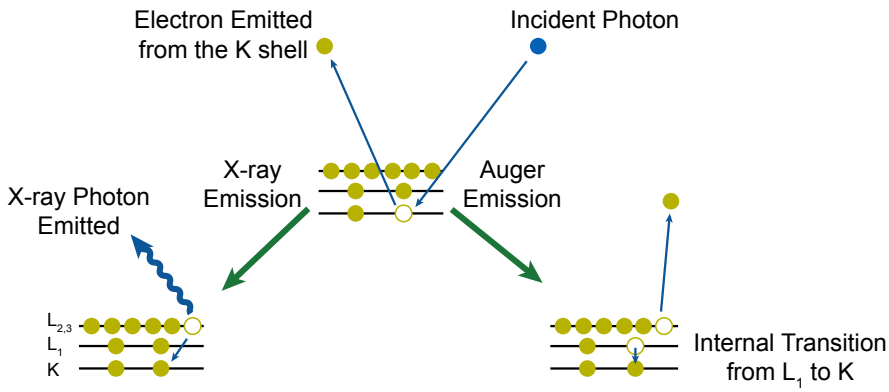

Figure 7: The ejection of a core-level electron by a high-energy incident photon leads to two competing processes: X-ray photon emission (left), and Auger electron emission (right).

Where σ is the total photoionization cross section, Ω is the solid emission angle, β is the anisotropy parameter, and θ is the angle between the direction of polarization and the emitted electron. It can be shown that this formula can also be used for randomly oriented nonspherical samples, such as free molecules or clusters ([59]).

In this description, the parameter β completely characterizes the angular distribution of electrons in photoelectron spectroscopy. In the case of photoionization of an s orbital in an atom described above, the β parameter will have a value of 2, with maximum emission parallel to the polarization direction and zero emission perpendicular to it. Generally, when β is positive, the emission tends to be in the direction of the polarization, when it is negative, it tends to be perpendicular to the polarization and is isotropic for β=0. Since the photoelectron differential cross section must be positive, β is bounded between -1 and 2, with the angular distribution becoming more anisotropic the further away from zero β goes. The angular distributions for some values of β are illustrated in Fig. 8. At a particular angle, the term $(3\cos 2\theta - 1)$ in Eq. 4 becomes zero, and the intensity is then proportional only to the total cross section, independent of the angular anisotropy. This angle is known as the magic angle and occurs at $\theta \approx 54.7°$ (see Fig. 8).

When electrons scatter elastically, the direction of the photoelectron is randomized to some extent, and the angular distribution becomes more isotropic, which means that the magnitude of the β parameter decreases compared to its original value. The more collisions an electron experiences before reaching the surface, the greater the reduction in anisotropy. As a result, it is possible, in principle, to estimate the distance from the surface to the point of origin of

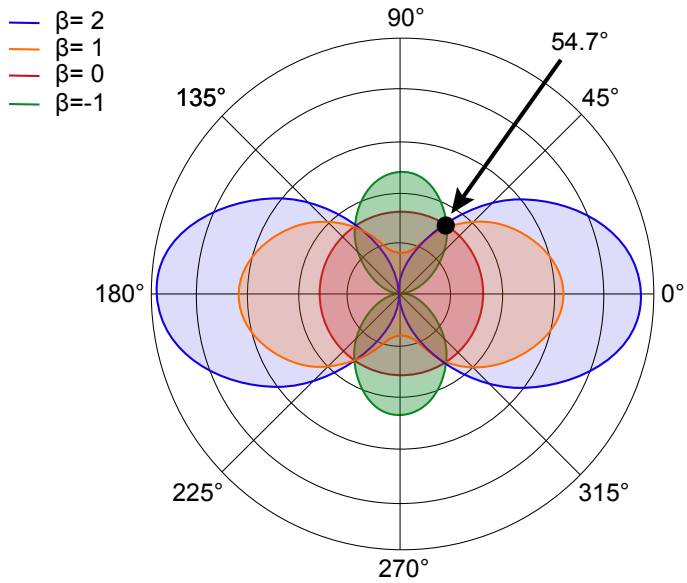

Figure 8: Polar diagrams illustrating the photoelectron differential cross section with four distinct values of β. The arrow indicates a "magic angle" 54.7°, at which the intensity becomes independent of β .

the photoelectrons on the basis of the amount of reduction in anisotropy. Even though the picture is quite complex, some studies have explored the depth distribution of surfactants and dissolved species in liquid-vapor interfaces, based on photoelectron angular distributions (PADs) from core levels[60].

Secondary scattering processes

For electron spectroscopy, the inelastic mean free path (IMFP) and the effective attenuation length (EAL) are critical parameters. The IMFP represents the average distance an electron travels before inelastic scattering occurs, while the EAL corrects for elastic scattering effects. The intensity of the photoemission signal is exponentially reduced as it travels through matter.

The IMFP of electrons is primarily determined by their kinetic energy of the photoelectrons and has a general pattern for many materials, including a minimum of about 5-10 Å in the 50-100 eV kinetic energy range and an increase toward both the low and the high energy sides, as shown in figure 9. This has the idea of a "universal" IMFP function common to all materials but with significant material dependence. This similarity means that the IMFP of electrons depends on their kinetic energy similarly for different materials, but the exact values may vary. This kinetic-energy dependence allows for depth-profiling experiments in

which the excitation energy is changed to vary the kinetic energy of the emitted photoelectrons from a specific electronic state. By changing the excitation energy, the depth from which the photoelectrons originate can be controlled, allowing for a deeper or shallower probing of the material. This behavior has also been shown for liquid water[61–64]. This makes electron spectroscopy methods highly sensitive to the surface of the material, as most detected electrons come from the first few atomic layers due to the short inelastic mean free path (IMFP) of the emitted photoelectron.

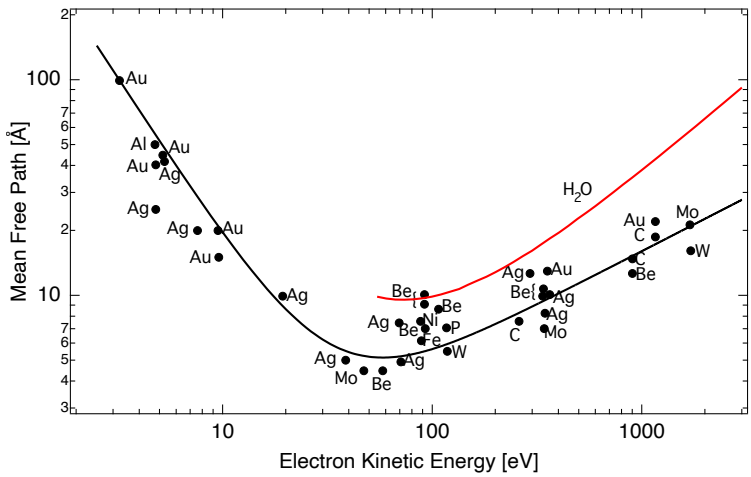

Figure 9: The inelastic mean free path of electrons in condensed matter follows a universal curve across various materials as a function of electron kinetic energy. The various data points (black symbols) are sourced from Somorjai,G. A. (1981)[65], with an approximate curve (black line) to illustrate the trend. The red line is a calculated IMFP curve for liquid water, Shinotsuka et. al. 2017[66].

The EAL complements the IMFP by accounting for elastic scattering effects. Elastic scattering occurs when photoelectrons change direction without losing energy. The EAL corrects for this phenomenon by considering both inelastic and elastic processes, giving a more realistic description of electron behavior within a material. In the context of this thesis, the EAL rather than the IMFP is used in the simulations presented in the chapter 2.7.

3.3 X-ray Absorption Spectroscopy (XAS)

X-ray absorption spectroscopies are widely used in synchrotron radiation facilities. These techniques are element-specific but are influenced by the chemistry and arrangement of nearby atoms. When a soft X-ray photon and an electron interact, the electron can be either emitted as a photoelectron or promoted to an unoccupied state. The photoabsorption normally increases in intensity

when the photon energy matches the ionization energy of the orbital being examined, forming an edge. The photoabsorption then drops with the photon energy, except for low-intensity fluctuations caused by interference between the photoelectron and its nearest coordination sphere, which provides information about the local geometry of the atom. This results in a spectrum consisting of pre-edge structures a few eV below the absorption edge and near-edge structures up to some tens of eV above the edge.

Considering the Beer-Lambert law (Eq. 1), the measurement is ideally performed in transmission mode, which can be considered the true method for measuring photon absorption. Other methods, such as fluorescence, electron, and ion yields, are approximations. In transmission mode, one observes a larger decrease in the intensity of transmitted light for higher photoabsorption cross sections, and this allows for the mapping of unoccupied levels by changing the photon energy.

The most direct method for observing X-ray absorption is therefore to measure the change in X-ray intensity before and after passing through the object of interest, as shown in the diagram presented in 29. However, this has a major limitation: the sample must be sufficently transparent to X-rays to obtain signal, which is often not the case for soft X-rays. For this method to be possible for liquid samples in this energy range, a 3D-printed nozzle was developed to achieve a flat, stable, and sub µm thickness to provide transparency for XAS measurements (more details in 6). Indirect methods of measuring absorption rate, requiring a decay such as fluorescence and Auger decay to occur before detection, are still possible and sometimes necessary even with this type of nozzle.

XAS can provide information on the orientation of a sample in addition to its chemical state. A common case is when an electron is excited from a 1s orbital in a light element (C, N, O). The probability of the transition will then depend on the alignment of the radiation polarization vector and the orbital into which the electron is excited[67]. By measuring the absorption spectrum at different angles between the polarization vector and a surface, XAS can, e.g. determine the tilt angle of surface adsorbates relative to the normal vector of the surface. The experimental setup used with the flat jet nozzles allows rotation of the liquid jet and can therefore be used to study alignment effects on liquid surfaces using XAS. The situation is not as straightforward as with solid surfaces due to the high roughness of liquid surfaces, but it is still a highly interesting development.

4 Experimental methods

In this chapter, the experimental setup that was used in this work is presented. In addition, the principles and features of synchrotron light sources, beamlines, and spectrometers are described.

4.1 Light sources for X-ray spectroscopy

The measurement of X-ray spectra requires a source of X-rays, for instance, laboratory X-ray sources, synchrotron light sources, and free-electron lasers (FELs). Laboratory X-ray sources are relatively inexpensive, simple, and compact. One of the main types of laboratory X-ray sources is sealed tube sources, but, while they are relatively inexpensive and easy to use, they have limited flux and essentially no energy tunability. In contrast, synchrotron light sources offer energy tunability for photons, and high brilliance at both high and low energies. Another type of radiation source is the Free Electron Laser (FEL) which has several advantages over synchrotron light sources[68], including coherence, even higher brilliance and ultrashort pulse duration due to the self-amplified spontaneous emission (SASE) process[69], while retaining wide energy tunability. However, FELs are also more complex and expensive to operate than synchrotron light sources, and their availability is currently limited.

Synchrotron facilities

Synchrotron facilities are large particle accelerators that produce intense beams radiation over a wide photon energy range (a few eV up to 10's of keV). These facilities are used for research in a wide range of scientific fields, including materials science, chemistry, biology, and physics. The MAX IV Laboratory, Sweden, which was used for the experiments in this thesis[70], is a fourth-generation (or diffraction-limited) synchrotron source[71]. It utilizes multibend achromats to achieve a small beam size (and hence high brilliance), and for longer wavelengths the diffraction contribution to the electron beam emittance is greater than the physical size of the beam, thus limiting the achievable brilliance. Fourth generation accelerators thus produce high-quality X-ray beams with high brilliance and coherence.

Synchrotron radiation (also known as *magnetobremsstrahlung* radiation) is electromagnetic radiation emitted when charged particles, such as electrons, are accelerated to relativistic speeds and forced to travel in curved paths by mag-

netic fields. When a charged particle moves in a magnetic field, it experiences a centripetal force that causes it to follow a curved trajectory, and the acceleration of the particle leads to emission of radiation.

Radiation produced by synchrotrons is several orders of magnitude more intense than that produced by conventional X-ray tubes or ultraviolet lamps, and therefore offers several advantages over conventional laboratory-based sources of X-rays. Firstly, the high photon flux allows more efficient data collection and can help to improve signal-to-noise ratios. Second, synchrotron radiation is highly tunable, meaning that it is possible to adjust the energy of the X-rays to match the energy levels of the atoms or molecules being studied, thus making it ideal for studying the electronic structure of materials, including the distribution of electrons within atoms and the nature of chemical bonding. Synchrotron radiation can be used with a range of spectroscopic techniques, including X-ray photoelectron spectroscopy and X-ray absorption spectroscopy - two techniques relevant to the work in this thesis, and fundamental for studying the electronic structure of materials.

In a synchrotron storage ring, the magnetic lattice consists of e.g. dipole magnets, used to bend the trajectory of electrons and to produce synchrotron radiation, as well as quadrupole and sextupole magnets, used to focus and correct aberrations. In modern synchrotrons, insertion devices such as undulators and wigglers are the main light sources, used to produce intense synchrotron radiation [72].

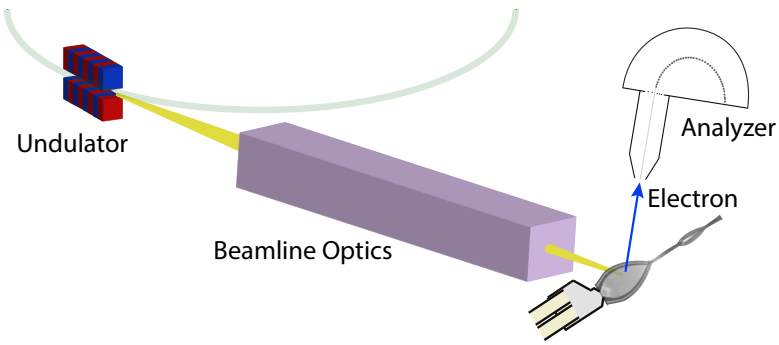

Figure 10: Simplified diagram of the experimental principle - a synchrotron light source, illustrating synchrotron radiation emission, beamline optics, the interaction of light with the sample and finally electron detection with a hemispherical analyzer.

Undulators are made up of a series of magnets that are arranged in a periodic pattern. When an electron beam passes through the undulator, the electrons are forced to oscillate back and forth as they pass through the magnetic field. The radiation emitted at these successive oscillations interacts, causing constructive interference for certain wavelengths of the radiation, called harmonics.

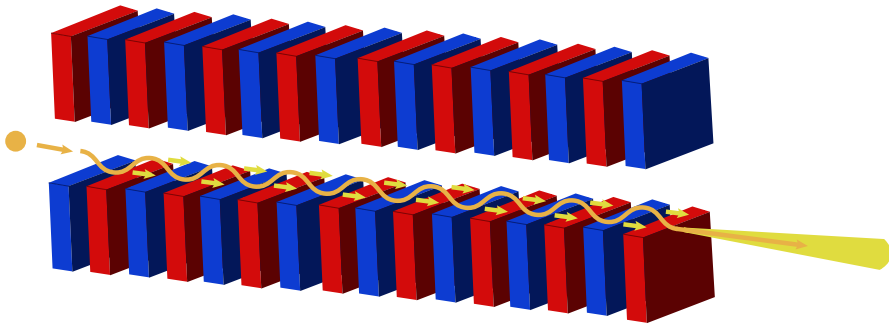

Figure 11: Schematic representation of the radiation emitted by the electron beam in a conventional undulator. The undulator consists of a series of alternating polarity magnets (represented by red and blue blocks) arranged linearly. Charged particles, such as electrons, pass through the undulator along the trajectory indicated by the orange line with arrows. As these particles travel through the spatially varying magnetic field, they emit radiation, represented by the yellow beam extending from one end of the undulator.

This results in a spectrum of quasi-monochromatic peaks, with the wavelength of the radiation for the first harmonic, the fundamental, emitted by the undulator given by the following expression:

$$\lambda = \frac{\lambda_u}{2\gamma^2}\left(1 + \frac{K^2}{2} + \gamma^2\theta^2\right) \tag{5}$$

where:

- K is the undulator parameter, defined as $K = \frac{eB_0\lambda_u}{2\pi m_e c}$, with B_0 being the peak magnetic field, e the electron charge, m_e the electron mass, and c the speed of light.
- λ_u is the undulator period.
- γ is the Lorentz factor, $\gamma = \frac{1}{\sqrt{1-\beta^2}}$, with $\beta = v/c$.
- θ is the observation angle relative to the direction of the electron beam.

The energy of the emitted beam is set by changing the spacing of the magnets (the "undulator gap"). In theory, an infinitely long undulator would produce completely monochromatic radiation in a series of harmonics defined by the magnetic field set by the undulator gap. The width of the undulator lines is given by the expression:

$$\Delta E = \frac{h\upsilon}{N} \tag{6}$$

where N is the number of periods.

One of the important characteristics of the radiation from undulators is brilliance. Brilliance is a measure of the intensity of light emitted by a source, taking into account the size of the source and the solid angle of the emitted light, as well as the bandwidth of the emitted light, which represents the range of wavelengths or energies present in the light. The higher the source's brilliance, the more photons it emits per unit time and per unit area, solid angle, within a given bandwidth, which is advantageous for scientific applications that require high sensitivity or rapid data acquisition.

Properties of synchrotron radiation which make it an excellent tool for scientific applications include high brilliance[2], a broad range of photon energies (from infrared to X-rays), a high degree of polarization [3], and pulsed temporal structure.

MAX IV Laboratory

MAX IV Laboratory is the Swedish national synchrotron radiation facility, located in Lund. MAX IV is a fourth-generation synchrotron, with a linear accelerator as an injector, and two storage rings for electrons. The 3 GeV ring has a circumference of 528 m and the 1.5 GeV ring has a circumference of 96 m[70], figure 12. MAX IV offers a broad range of photon energies and a wide variety of instruments to the international research community. In total, MAX IV currently has 16 beamlines covering a wide range of X-ray photon energies from 4 eV to 40 keV, which include various measurement techniques such as X-ray spectroscopy, scattering, diffraction, and imaging for a multidisciplinary

[2]Number of photons emitted per second, per unit area of the source, per unit of solid angle, and for a bandwidth of 1/1000 of the photon energy.

[3]For bending magnets, the light is linearly polarized in the plane of the electron orbit and elliptically polarized outside this plane. For planar insertion devices, the oscillations tend to cancel out the circular contributions of the left and right hand.

user community. At MAX IV Laboratory, XPS experiments on liquid jets are possible using photon energies up to 2 keV.

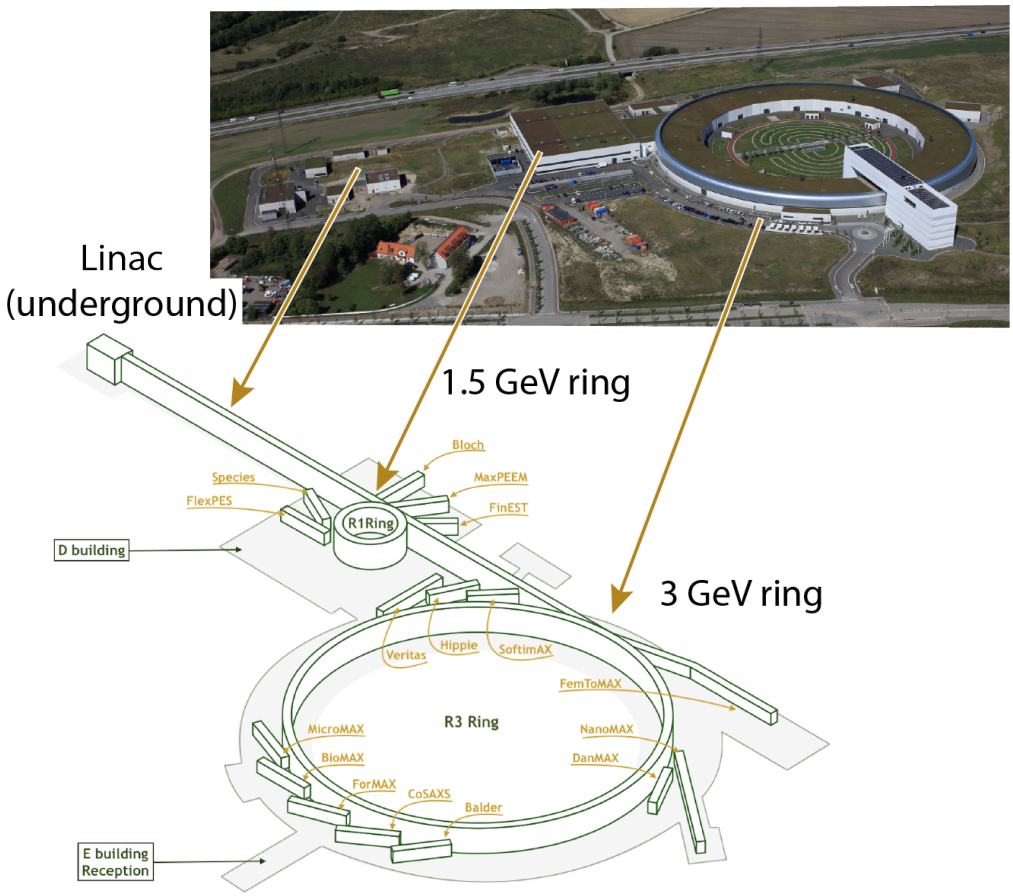

Figure 12: Overview of the MAX IV Laboratory layout and panorama of main facilities on the top. The 3 GeV ring spans 528 meters in circumference, while the 1.5 GeV ring measures 96 meters. The linear accelerator (approximately 300 meters) is situated underground. *Adapted from a figure provided by Anicée Guglielmi.*

4.2 FlexPES beamline

The main components of a typical soft X-ray beamline are the light source (such as an undulator or a bending magnet), a focusing mirror, a monochromator, an exit slit, and a refocusing mirror. Beamlines are designed to meet the specific requirements of the measurement techniques that are offered at that beamline, and important parameters to consider are energy range, photon flux delivered by the source, polarization characteristics, and the spot size at the focus point.

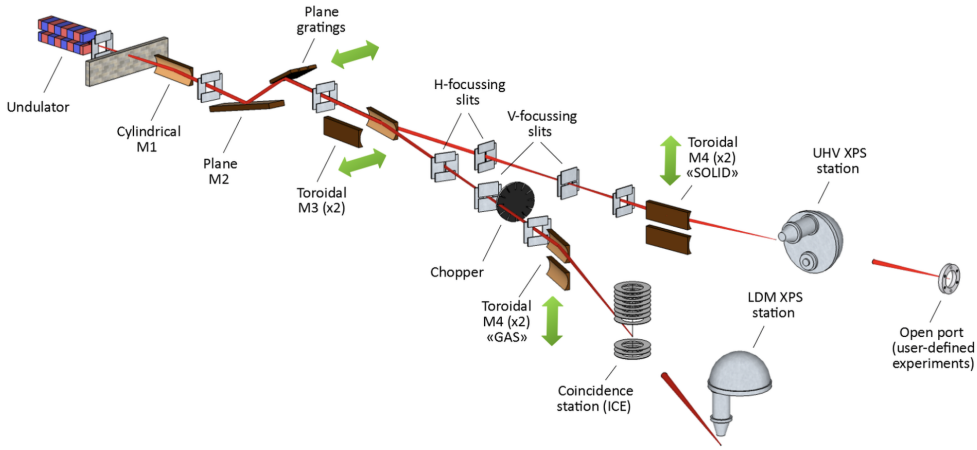

Figure 13: Schematic layout of the FlexPES beamline [73] (reproduced under open access with a Creative Commons CC-BY 4.0 license).

For the research presented in this thesis, the FlexPES beamline at MAX IV Laboratory was used. FlexPES is an undulator beamline with linear horizontal polarization and operates in the soft X-ray regime with a photon energy range of 40 to 1500 eV [73]. The beamline has two branch lines, each equipped with a double-striped toroidal refocusing mirror which allows the beam to be focused at two different points along each branch. As a result, the beamline can deliver a focused or defocused beam to two different endstations in each branch. The endstations are:

- Surface and Material Science (SMS) Branch: EA01: Permanent UHV endstation, for studies of on-surface processes. EA02: Open port reserved for user-provided endstations, 2.5 m downstream from EA01.
- Low-Density Matter (LDM) Branch: EB01: Ions in Coincidence with Electrons (ICE) endstation, for photo-stimulated fragmentation processes in gas-phase atoms, molecules, and clusters. EB02: The Low Density Matter Photoemission End Station, for photoelectron and X-ray absorption spectroscopy studies on gas particles, free clusters, and liquid jets, as well as surfaces and thin films. The experiments presented in this thesis were carried out at EB02.

Figure 13, shows a schematic overview of the FlexPES beamline [73]. The essential parts of the FlexPES beamline are:

Table 1: Photon Flux and Beam Characteristics at FlexPES beamline

Exit slit	Photon flux on the sample	Energy
10 µm	10^{12} photons/s	150 eV
10 µm	10^{10} photons/s	1000 eV
Energy resolution	**Energy**	
≈3.5 meV	60 eV	
≈100 meV	1000 eV	
Beam focus size	**Exit slit**	
≈100 x 130µm (VxH)	50 µm	

- The M1 cylindrical mirror which deflects the beam horizontally and collimates it vertically.

- A plane-grating monochromator, operating with collimated light in the vertical (dispersive) direction, a so-called collimated plane-grating monochromator design (cPGM). It is a modified Zeiss SX700, with the plane mirror (M2) and plane grating independently rotatable, and with the possibility to choose between two gratings: 1221 lines/mm and 400 lines/mm.

- A switching mirror, allowing switching between the two branches by the selection of one of two toroidal focusing mirrors (M3). M3 focuses the light at the exit slits of each branch.

- A refocusing mirror (M4), which is a toroidal mirror that focuses the synchrotron beam from the exit slits in a spot at the endstation.

All optical surfaces are Au-coated; M1, M2, and the grating are water-cooled, while M3 and M4 are not, due to the reduced heat load after the dispersion of light in the monochromator. Typical flux, resolution, and spot size figures for FlexPES are presented in Table1.

XPS on liquid samples

The hemispherical electron analyzer (introduced in section 3.1) allows the measurement of electron energy with high resolution. A typical hemispherical analyzer setup for XPS studies of liquid jets (Fig.6) is composed of an experimental chamber (where the synchrotron radiation interacts with the sample) which is separated from the hemispherical analyzer instrument via an opening in a small skimmer. The sample to be investigated is placed close to this entrance skimmer so that the electrons to be investigated can enter the analyzer. The instrument has an electrostatic lens that focuses the electrons to be measured through the analyzer entrance slit and into the hemispherical analyzer. The two concentric charged hemispheres generate an electrostatic field that serves to deflect the electrons as a function of their kinetic energies. After travelling through the analyzer, the electrons are detected with a position sensitive detector.

When analyzing cylindrical liquid jet samples, care must be taken to ensure that the liquid laminar part of the liquid jet (see Fig.14) is positioned to intersect the radiation from the beamline 2-3 mm after leaving the nozzle, before the jet breaks up into droplets. When measuring with liquid flat jets, we utilize the first sheet immediately after the nozzle opening. In the FlexPES liquid jet setup, the rod holding the nozzle is mounted on a rotary stage, enabling variations in the angle between the liquid sheet surface and incoming radiation.

XPS data analysis for liquids

A practical approach to XPS data analysis includes the following steps:

1- Data collection: The first step is to collect high-quality XPS data using appropriate spectrometer settings.

2- Peak fitting to obtain binding energies and peak areas.

3- Background subtraction from the X-ray photoelectron spectrum.

4- Quantification of the relative chemical elements of the sample based on the areas of the XPS peaks.

5- Examination of core-level shifts to determine the chemical state of the elements in the sample.

6- Assignment of the chemical state of the elements in the sample based on the XPS data, taking into account other information such as the sample environment

and other data sets.

The goal of XPS data analysis is to learn more about the sample under investigation. An X-ray photoelectron spectrum often exhibits photoemission peaks sitting on a background of inelastically scattered electrons. The peaks are made up of one or more components, and their appearance depends on various phenomena, including instrumentation geometry. A Voigt function, which is a convolution of Lorentzian and Gaussian functions,[74] is often used to fit the peaks for nonconducting samples and has been extensively used for the data analysis presented in this thesis. The typical approach to XPS analysis involves subtracting the background and doing a least-squares curve fitting of the spectral components, using appropriate line shapes.

In this thesis, the SPANCF fitting routine package, created by Edwin Kukk for Igor Pro[75], was used to fit photoemission lines. The script fits a photoelectron spectrum by combining a linear background, other optional nonlinear backgrounds, and a variable number of photoemission lines. The photoemission lines are defined by parameters such as the energy position, intensity, Lorentzian width, Gaussian width, and asymmetry. The fit can be constrained by locking or by linking certain parameters, for example, two lines can be separated in energy by a fixed value or two features can have a constant intensity ratio.

Because of vibrational excitations in the ionic state, distinct vibrational progressions are often seen in molecular gas-phase photoelectron spectra. In liquids, the vibrational progression is typically hidden because of other broadening mechanisms, for instance, small chemical shifts caused by the changing surroundings. As a result, the vibrational profile is often observed to be broad and undefined compared to a gas-phase sample.

Another feature which is much more prominent in condensed sample spectra compared to gas-phase data is the background created by secondary electrons. This strong background in practice prevents measurements of photoelectron signal with too low kinetic energies for liquid samples.

Experimental conditions, such as the photon bandwidth, determined mainly by the beamline slit size, and the resolution of the electron spectrometer, defined by the pass energy and the spectrometer entrance slit size, affect the Gaussian width. The aim is typically to design experiments so that the width of the spectral features is primarily determined by inherent factors. For instance, in studies of Auger electron spectra, where photon resolution does not influence the measurement, the monochromator slit can be opened to increase flux on the sample.

In addition to Gaussian broadening, the Lorentzian contribution to the line width arises from the finite lifetime of the excited state, known as lifetime broadening. According to the uncertainty principle, the energy uncertainty and the lifetime of the state are inversely related. This results in a Lorentzian line shape, characterized by its distinct tails that extend from the peak. The Lorentzian profile is mathematically described by the function:

$$L(\nu) = \frac{1}{\pi} \frac{\frac{\Gamma}{2}}{(\nu - \nu_0)^2 + \left(\frac{\Gamma}{2}\right)^2}$$

where ν is the frequency, ν_0 is the central frequency, and Γ is the full width at half maximum (FWHM), which is related to the lifetime of the state. While this type of broadening is homogeneous, affecting all molecules or atoms equally, the actual lifetime broadening varies between different elements and core levels, and values are typically found from literature[76].

4.3 Liquid jets for spectroscopy measurements

Understanding the chemical and electronic properties of liquid surfaces and interfaces is crucial for a wide range of applications, such as catalysis, electrochemistry, or biointerfaces. For example, in catalysis, the activity and selectivity of catalysts can be strongly influenced by the surface chemistry and morphology of the active sites, which can be probed by XPS. In electrochemistry, the charge transfer kinetics and reaction mechanisms at electrode surfaces can be studied by XPS, which can provide insight into the nature of the adsorbed species and their interactions with the electrode. In biointerfaces, XPS can be used to investigate the composition and structure of biological membranes, proteins, and other biomolecules at interfaces with synthetic or natural materials. The information obtained from the XPS measurements can help design and optimize new materials and devices for various applications. Indeed, X-ray spectroscopy (and X-ray scattering) is widely utilized in various scientific disciplines and the effectiveness of the technique often hinges on the stability of the sample delivery system.

Cylindrical microjets

Over the past thirty years, cylindrical liquid jets (Figure 14) have often been used as sample injection systems in experiments designed to analyze samples

in solution and suspension. In particular, this sample delivery method has been demonstrated to be a highly effective and popular approach for liquid XPS measurements. Its defining characteristics include well-defined geometry, stability, reproducibility and sample renewal capabilities (which removes the risk of radiation damage and minimizes surface contamination). These well-developed modern cylindrical jet systems offer several advantages, including a manageable vacuum load if the jet is sufficiently small and a rapid decrease in vapor pressure due to the curvature of the jet (in contrast to the case for a flat jet). In addition, it is possible to align the cylindrical jet with the X-ray beam in order to maximize the signal-to-noise ratio while minimizing the background signal from the gas phase[77]. These jets can also be cooled to reduce thermal damage and evaporation during measurements.

However, cylindrical jets have some limitations for XPS measurements. The major limitation is the curvature of the sample surface, which results in the absence of a defined surface orientation. Furthermore, issues related to volatility (vapor pressure) and viscosity are present, although these are also common to flat jets. It is important to note that the limitation in probing depth in XPS (a few nanometers at most) is not inherent to the jet itself but rather to the sample (the liquid) and the probing method (the X-rays and the electrons).

In addition, some general limitations for liquid jet measurements exist (regardless of the type of liquid jet used). Soft X-ray XPS experiments using liquid jets require a relatively high vacuum environment, both for the effective transport of the X-ray photons to the interaction region and to avoid contamination and ionization effects in the data. Residual gases or vapors in the vacuum chamber or the presence of contaminants or impurities on the surface can also affect the X-ray photoelectron spectra by introducing spurious peaks or background signals.

The experimental setup for generating liquid jets using GDVN nozzles, for example, typically involves a liquid reservoir, a high-pressure pump, a nozzle, a gas, and a vacuum chamber. The liquid is pumped from the reservoir to the nozzle at a controlled flow rate, in which the gas flow and aperture determine the jet velocity and diameter. The gas chamber surrounds the nozzle and provides a shearing gas flow that helps stabilize the jet and prevent its breakup into droplets. The gas pressure and flow rate can be adjusted to control the jet stability and break-up mode.

The characteristics of the jet, such as stability, diameter, and velocity, depend on several parameters, such as the nozzle geometry (diameter, length, shape), the liquid properties (density, viscosity, surface tension), and the operating con-

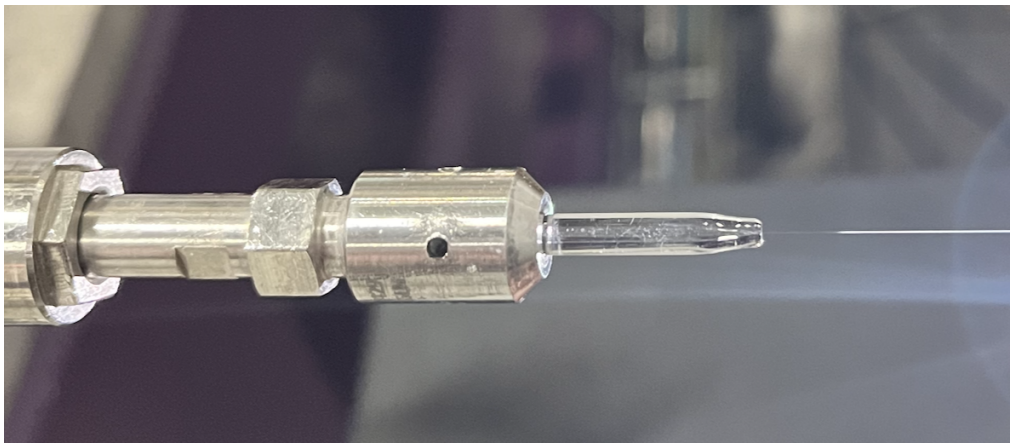

Figure 14: Photo of a cylindrical liquid jet produced using a commercially purchased nozzle (AdMiSys GmBH). The laminar part of the liquid jet is visible close to the nozzle opening (the darker shaded part of the flow).

ditions (liquid flow rate, gas pressure, gas flow rate). For example, in the case of GDVN:s, the gas flow rate has a greater effect on the jet diameter than the liquid flow rate. For Rayleigh jet types [4], only the nozzle tip influences the jet diameter, while the flow primarily affects the jet length and speed. However, these changes can also impact the stability and breakdown mode of the jet.

The stability of the cylindrical jet is influenced by several factors, such as the surface tension of the liquid, the viscosity of the liquid and gas phases, and the aerodynamic forces acting on the jet. For example, increasing the surface tension or viscosity of the liquid can increase its resistance to breakup by Rayleigh instability. Similarly, increasing the gas pressure or flow rate can increase its resistance to breakdown by aerodynamic instability [78,79].

Liquid flat jets

Despite their widespread use, cylindrical liquid jets present several challenges that limit their use for a variety of experiments [77,80]. For example, most cylindrical jets used in photoelectron spectroscopy have diameters of 25 µm or larger, while GDVN has the most standard nozzles in a range of 5 µm, which is too thick for soft X-ray transmission spectroscopy, where the transmission length is only a few micrometers. [50,52] Additionally, the thickness of a cylindrical jet varies significantly across the focal spot of the X-ray beam, making it diffi-

[4] Rayleigh jets refer to slender liquid streams formed when a liquid is pushed through a small opening under significant pressure. These jets owe their name to Lord Rayleigh, who investigated the instability leading to their fragmentation into droplets.

cult to accurately determine the X-ray path length through the sample.[81] This variability hinders the precision of absorption measurements and can affect the intensity of detected photoelectrons, leading to uncertainties in photoelectron spectroscopy analysis.

In contrast to cylindrical jets, liquid flat jets, although currently less prevalent, are better suited to certain research applications that require a thin and wide liquid surface with controlled thickness and orientation. Conveniently, liquid flat jets can be generated using microfabrication techniques or by implementing specialized nozzles that produce a planar liquid sheet, and they are suitable for use under vacuum or Near Ambient Pressure (NAP) conditions, which are experimental settings close to atmospheric pressure. Such flat sheet jets provide a large (micrometer) uniform liquid surface that can be used to study the dynamics, structure, and reactivity of liquid surfaces and interfaces under various external stimuli, such as shear flow, electric fields, or surface waves. They also allow for the study of liquid surfaces with different orientations and crystallographic planes[82,83].

The motivation for developing a liquid flat-jet system is to overcome the experimental limitations of cylindrical jets such that they can be employed for new types of experiments. For some applications, flat sheet jets offer significant advantages over cylindrical jets due to their nearly planar flow characteristics.[50,77,84] As discussed above, cylindrical jets are too thick for soft X-ray transmission measurements, they exhibit varying optical path lengths within the liquid, and possess a macroscopic curvature of the liquid surface, complicating the study of surface orientation effects.

One of the principal benefits of utilizing a flat jet to a cylindrical jet is its ability to generate targets of an exceptionally thin liquid phase. Specifically, flat jets allow for more precise control over the thickness of the liquid phase, ensuring uniform sample thickness. Flat jets also offer a versatile platform for conducting unique liquid-phase experiments that are not possible with single cylindrical jets. For example, researchers can generate two co-flowing liquid-jet sheets with a shared interface in a vacuum[85]. Each surface of these sheets, facing the vacuum, represents one of the solutions, which allows for face-sensitive detection using photoelectron spectroscopy. Several recent studies have explored alternative sample delivery systems to enhance the quality of X-ray scattering and spectroscopy experiments on liquid phase samples, and flat liquid sheets have been identified to have immense potential to improve these experiments.[51–53,78,79,86–93].

For instance, Watanabe et al.[86] explored the use of liquid microjets for X-ray absorption spectroscopy, which allows for precise measurements and minimizes

sample consumption. Ganan-Calvo et al.[87] focused on electrospray techniques for creating fine droplets of liquid samples, particularly useful for mass spectrometry. Klebniczki et al.[88] investigated gas dynamic virtual nozzles (GDVNs), which create fine liquid jets by focusing a liquid stream with a co-flowing gas, commonly used in serial femtosecond crystallography.

Small and Wide Angle X-ray Scattering (SAXS and WAXS), providing nearly planar flow and uniform sample thickness. Fondell et. al[52] explored liquid sheet jets, offering a large surface area and uniform thickness for X-ray scattering and spectroscopy. Galinis et al.[49] focused on microfluidic devices for precise control over the flow and mixing of small liquid volumes. DePonte et al.[92] examined liquid droplet injectors for delivering samples to X-ray free-electron lasers, producing synchronized streams of droplets. Koralek et al.[53] explored aerosol-based sample delivery systems, useful for volatile or sensitive samples. Schulz et al.[93] focused on microjet mixing techniques for creating homogeneous samples. Knoska et al.[51] investigated ultracompact liquid jet systems for delivering samples to X-ray free-electron lasers. Vakili et al.[79] explored mixing jets for creating homogeneous liquid samples.

Creating a liquid flat jet is a complex process that requires precise control over fluid dynamics. The key components involved in this process include the fluid delivery system, the jet formation device, supporting structures, and characterization equipment. The fluid delivery system consists of pumps, filters, flowmeters, and pressure gauges. Pumps precisely control the flow rate and pressure of the liquid, while filters remove impurities that could affect jet formation. Flow meters measure and regulate liquid flow, and pressure gauges monitor system pressure. In addition, characterization equipment such as high-speed cameras, interferometry (for measuring jet thickness and refractive index), and spectroscopy (for analyzing liquid composition and properties) is essential for understanding liquid flat jet behavior. Moreover, hardware such as support structures to stabilize the jet during formation and experimentation, for example, jet holders, provide stability and specialized chambers for analysis.

Liquid flat jets can be broadly categorized into two main types, collision-based or sheet-forming because of the nozzle design. Collision-based jets form when two or more cylindrical jets collide, resulting in a flat sheet. Precise control over jet velocity, angle, and distance is critical for these jets, which find applications in microfluidic systems. Alternatively, sheet-forming nozzles directly create a flat sheet without the need for collisions, i.e. the flat-sheet generation is based solely on the nozzle design. However, achieving uniform thickness and stability can be challenging.

Collision-based liquid flat jets

One promising approach to generate collision-based sheets involves generating liquid flat jets through the collision of two Rayleigh jets.[94,95]. However, the colliding system methodology requires the use of conventional liquid Rayleigh nozzles, which require meticulous alignment of the nozzle pair and relatively elevated liquid flow rates. This can prove challenging in the context of scarce or valuable samples as well as in maintaining optimal vacuum conditions throughout the operational process.

However, the interaction of two cylindrical jets can be manipulated by applying different bias potentials to each jet.[85] This technique can create a potential gradient between the two solution phases, which is useful for experiments investigating electrochemical processes or charge transfer mechanisms. The ability to control and vary the potential gradient provides researchers with a powerful tool to explore a wide range of phenomena in liquid-phase systems. Stemer et al.[85] have recently developed this method, and adapted it for photoelectron spectroscopy experiments in a NAP XPS setup.

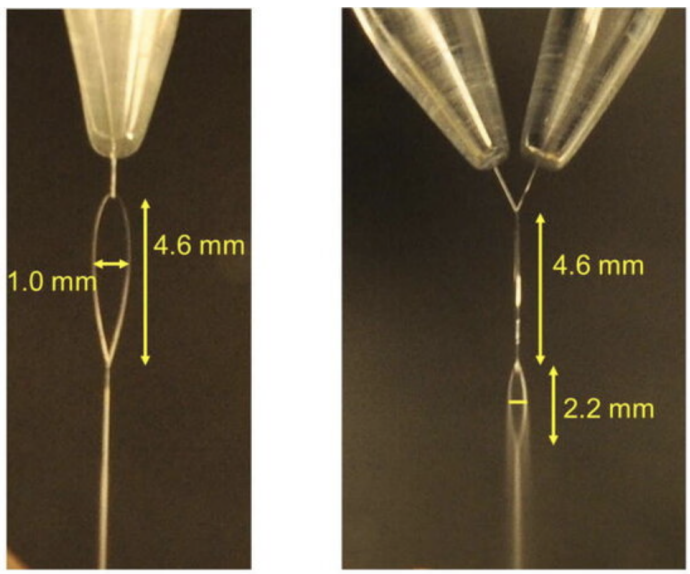

Figure 15: Image captures a liquid flat jet viewed from two perpendicular angles, revealing the creation of a stable initial sheet and the emergence of small droplets in the second sheet. (Image "A liquid flatjet system for solution phase soft-x-ray spectroscopy," by M. Ekimova, W. Quevedo, M. Faubel, P. Wernet, and E. T. J. Nibbering, Structural Dynamics, Vol. 2, No. 5, p. 054301, (2015); used in accordance with the Creative Commons Attribution (CC BY) license)[50]

An alternative approach used by Ekimova et al.[50] used two cylindrical glass nozzles with a diameter of 50 µm, positioned at an angle of 48°, with respect to each other, and a distance of 0.8 mm between the exits of the nozzle (see Figure 15). This setup allowed them to form a liquid sheet approximately 4.6 mm long and 1.0 mm wide, with a thickness ranging from 1.4 µm to 3 µm depending on the position. To achieve an optimum stable sheet, a liquid flow rate of around 5.7 - 6 ml/min was required. The pressure in the main chamber was approximately 10^{-5} mbar, with a working pressure of 10^{-3} mbar.

Fabricated flat jet nozzles

In 1989, Watanabe et al.[86] introduced a novel jet nozzle capable of producing ultrathin liquid sheets with a thickness of 3.5 µm. This nozzle design features a stainless steel tube compressed with a rectangular cross section (200 µm x 5 mm), incorporating a trapezoidal groove on one side of the tip and a conical hole on the other side, figure 16. This design effectively produces a flat liquid sheet by impeding the wedge-shaped liquid flow generated by the tapered channel from both edges. The nozzle is specifically designed to work with low-viscosity fluids, such as a mixture of ethylene glycol and ethanol. The liquid sheets generated with this nozzle exhibit extremely high optical quality, representing a significant advancement in the field of femtosecond pulse dye lasers.

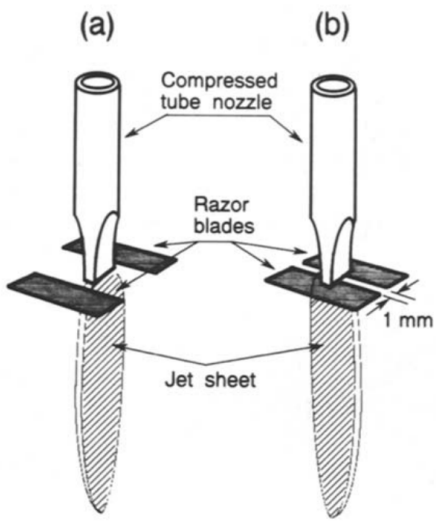

Figure 16: Jet nozzle a) before liquid flow obstruction by two razor blades, representing the conventional jet flow, and (b) with a new flow achieved by blocking the liquid flow using the same blades. (Copyright license n. 5861251116084)[86]

In another study, Galinis et al.[90] developed a novel method for creating thin liquid sheet jets in a vacuum environment. They achieved this by using custom 3D-printed nozzles designed to guide the liquid streamlines to collide within the nozzle at a selected angle. A flat sheet jet with dimensions of 260 x 30 µm dimensions was formed upon exiting the nozzle. The nozzles were fabricated using high-resolution (0.2 µm) two-photon 3D-printing and an IP-S polymer material. Isopropyl alcohol was used as the working fluid during the testing. The resulting liquid sheet jets had a thickness ranging from 1 µm to 5 µm and exhibited extremely high optical quality and flatness.

Another new development has opened up possibilities for generating liquid sheets using gas compression in a microfluidic chip.[53] Here, sheet jets are formed by two gas streams compressing a central liquid flow into stable and thin sheets. The flat jet thickness can be determined by interferometric or mid-infrared transmission measurements under atmospheric pressure and by soft X-ray transmission measurements under vacuum conditions, where the thickness of the first liquid sheet is found to vary around a few nm to µm scale, depending on the transverse and longitudinal position in the liquid sheet. In a related study, Shen and Poulikakos[96] used holographic interferometry to measure the thickness variation of a liquid sheet formed by two impinging jets, finding that the thickness distribution can be accurately captured in real-time and further explored the thickness variation along and across liquid sheets, providing detailed insights into the dynamics of liquid sheet formation. Moreover, Hoffman et al.[97] demonstrated that microfluidic liquid sheets can serve as large-area targets for high repetition X-ray free-electron lasers (XFELs). Buttersack et al.[84] presented spatially resolved measurements of the temperature and thickness of thin planar liquid water jets in vacuum, highlighting the influence of environmental conditions on liquid sheet properties.

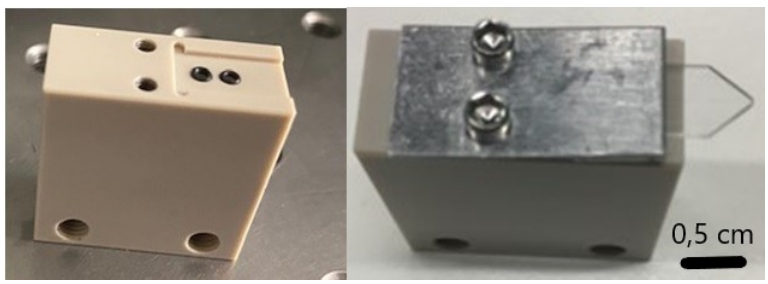

Figure 17: Flat sheet interface for the commercial micronit nozzles.

Commercial gas-dynamic nozzles are available on the market. The Micronit Micro-technologies BV[53] nozzles feature three microfluidic channels within a borosilicate glass chip. The fabrication process of these nozzles involves standard hard lithography techniques, resulting in a hydrophobic coating on the chip's surface. Symmetric wafers are bonded together to create cavities that serve as liquid channels. The chip comprises two 50 µm diameter channels intersecting a central 20 µm channel at angles of $\pm 40°$ before the exit opening. In the setup presented in this thesis, the MC was assembled in a two-channel interface, as depicted in Figure 17. It functioned as a dynamic gas flat sheet, where a high-velocity helium gas sheath accelerated and compressed the liquid within the central channel.

5 Results and Experimental Outcomes

This chapter presents the principal results of this thesis. A significant part of this study involves the design, characterization, and implementation of a 3D-printed flat sheet nozzle, which facilitates the advancement of liquid-phase soft X-ray spectroscopy studies by providing a planar surface geometry and micro-thin-sheet jets. The successful implementation of a rotary setup for XPS and transmission-mode XAS measurements using a flat jet has expanded the capabilities of liquid-phase spectroscopy at MAX IV Laboratory.

5.1 Nozzle designs for liquid flat jet

3D-printing technology offers several benefits over conventional manufacturing methods, including the ability to generate intricate geometries with high accuracy, low cost, and rapid turnaround time. Additionally, 3D-printing enables quick prototyping and iterative design optimization, facilitating improvements in the performance and efficiency of the nozzle system.

To develop a compact flat sheet nozzle for the FlexPES beamline, we employed 3D-printing technology to customize and create various nozzle designs tailored to specific experimental requirements, allowing for more complex flow behavior. The standardization of the flat sheet design was implemented to address the need for consistent and reproducible results, which is crucial to investigating more challenging scientific questions.[51,79] The importance of standardization in the design of the nozzle ensures uniformity in the flat sheet design, achieving consistent flow characteristics, which are essential for reliable experimental outcomes. This standardization also facilitates the comparison of results across different experiments and setups, thereby advancing our understanding of complex fluid dynamics [5]. From a technical viewpoint, it is critical to correlate the dimensions of the flat sheet with the flow of liquid and gas in various experimental configurations, particularly when examining liquid samples using analytical techniques. The relationship between these parameters influence factors such as sample concentration, exposure time, and data quality.

Figure 18 shows an image of one of the 3D-printed nozzle designs, developed in relation to this work. Details regarding nozzle assembly during the experiment can be seen in **Paper II**. A variety of nozzle designs have been developed and studied, and the one that presented the most stable jet has been chosen for implementation at the FlexPES beamline. In the collision region, seen in the figure,

[5] *(J. Valerio et.al. in preparation)*

the gas and liquid channels converge, creating the sheet surface. The behavior of the nozzle has been studied under varying gas flow rates, and these studies show the importance of maintaining a specific range for stability. In **Paper II**, the capability of the nozzle to form stable liquid sheets is demonstrated.

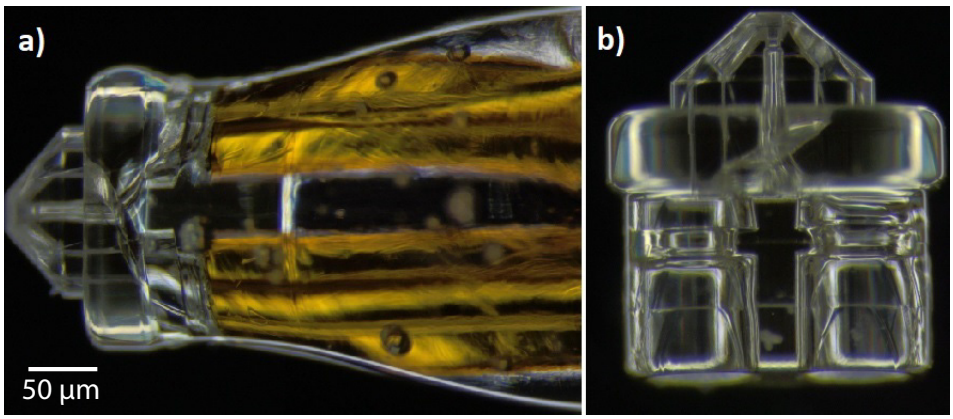

Figure 18: 3D-printed nozzle design. (a) Nozzle assembly with two capillaries. The upper capillary is responsible for introducing the liquid sample, while the lower one is connected to the helium gas line.(b) Magnified view, highlighting the design of the 3D-printed nozzle. An Olympus SZX16 microscope and UC90 camera were used to capture the image.(**Paper III**)

5.2 3D-print nozzles at EuXFEL

To develop the 3D-printed nozzles intended for this collaboration between MAX IV and EuXFEL, the advanced infrastructure at EuXFEL was used. To create the 3D-printed nozzle, a Photonic Professional GT (Nanoscribe GmbH, Karlsruhe, Germany), a high resolution three-dimensional (3D) printer, was used. This printer can create structures on a nanometer scale using the Two-Photon Polymerization (2PP) process. The operating principle is based on the use of a high-powered laser that is focused into a photo-resist material, IP-S resin, using an objective lens (20x), which concentrates the intense laser light in a small region. This triggers a non-linear light absorption process, where the resin molecules simultaneously absorb the energy of two photons, that solidifies the material locally, resulting in structures with a resolution of sub-300 nm, as represented in figure 19. By moving the photo-resist relative to the laser, or vice versa, using galvanometer motors producing a precise and controlled motion, complex 3D high-resolution structures can be printed. As a target, one droplet of a UV-curable photoresist IP-S resin is added onto a glass slide in which one side is coated with a layer of Indium Tin Oxide (ITO). The ITO-coated glass makes the glass slide highly conductive and transparent.

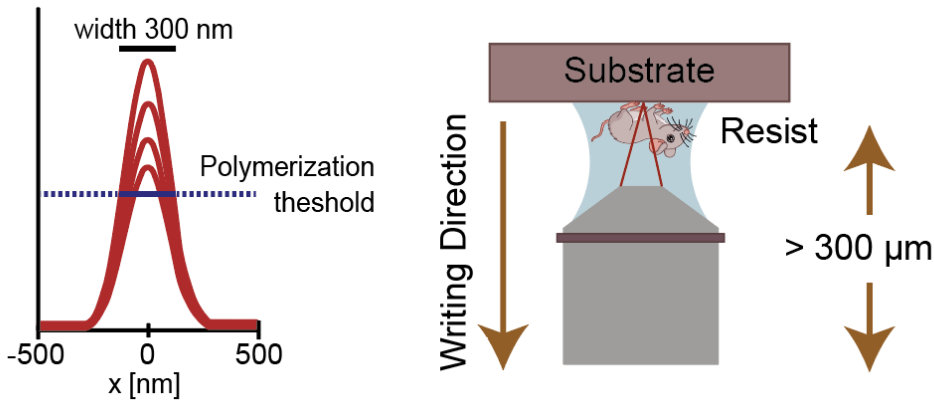

Figure 19: Schematic representation of the NanoScribe 3D-printing process. (a) The diagram illustrates the polymerization threshold within a 300 nm width, and (b) shows the writing direction starting on the substrate and moving away from the surface, with a limit for the height of 300 µm above the substrate.

Figure 20 illustrates the key steps involved in the nozzle fabrication process. Panel (a) depicts the workspace setup for the printing operation. In (b), the resin used for the production of the nozzle, the formation of droplets before printing, and an array of successfully printed nozzles, is shown. The revealing process, before the curing of the photoresist resin, is presented in panel (c); more details are given below. Panel (d) provides a microscopic view of a cleaned and cured GDVN nozzle.

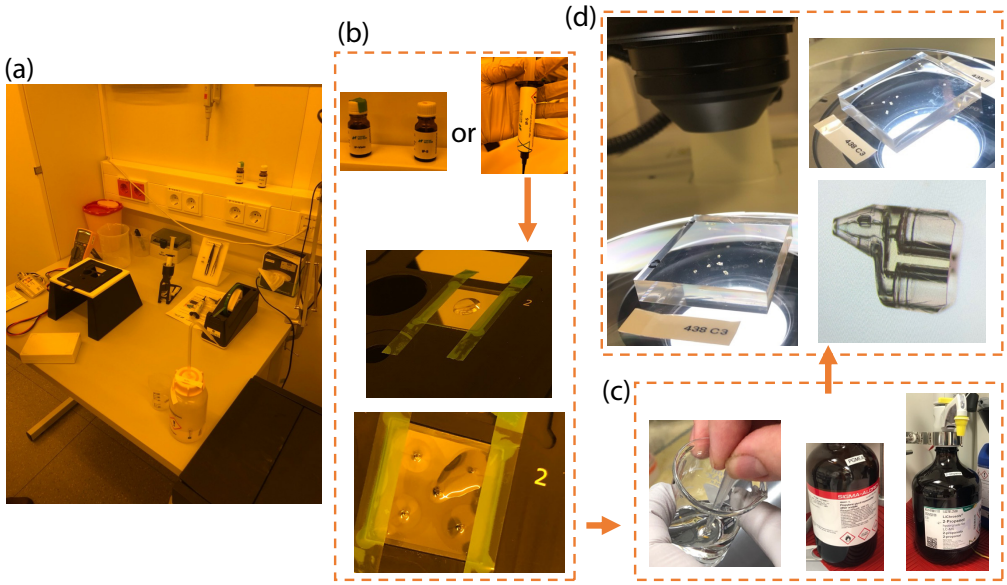

Figure 20: Summary of nozzle fabrication (a) Experimental setup for nozzle fabrication. (b) Top: Resin used for nozzle production. Middle: Resin droplet before 3D-printing. Bottom: Array of five printed nozzles. (c) Cleaning process of the printed nozzle before photoresist curing. (d) Microscope images of a cleaned and cured GDVN nozzle.

One of the nozzle designs presented in this thesis is illustrated in Figure 21, where two-photon polymerization (2PP) has been used to fabricate a 3D structure capable of producing high quality liquid sheets. The nozzle consists of three primary components: the inlet ports, an intermediate transition zone, and the outlet section.

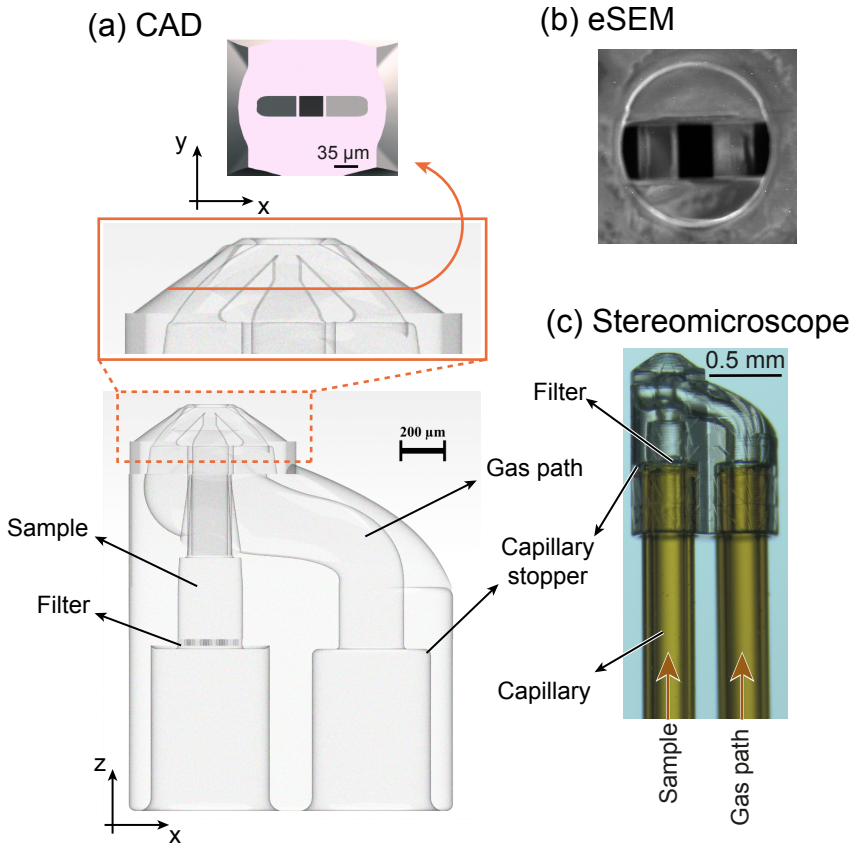

Figure 21: (a) 3D rendering of a gas-accelerated micro-sheet CAD model. (b) Environmental scanning electron microscope (eSEM) image of the nozzle's exit channels. (c) 3D-printed nozzle with two assembled capillaries: the left one for liquid sample insertion and the right one connected to the He gas line. Captured using an Olympus SZX16 microscope and UC90 camera.**(Paper II)**

The nozzle's outlet channels the sample fluid through ducts with a quasi-rectangular profile, as depicted in Figure 21a,b. This geometry, combined with gas compression, results in a thin, broad liquid sheet comparable to those generated by commercially available glass nozzles (Micronit®)[53]. The 3D-printed nozzle consistently produces stable jets with high reproducibility, demonstrating successful operation in 80% of the fabricated devices.

Both the gas and liquid channels (Figure 21 a and c) have an initial inner diameter (ID) of 365 µm. This is followed by a 540 µm section that reduces the ID to 200 µm, forming a capillary restrictor. The final channel segment is 330 µm long with a 100 µm diameter for the sample flow. A 40 µm pitch mesh filter is integrated within the sample channel to prevent particle contamination[51]. The

central section features a divided gas pathway that converges at a 45° angle, intersecting the liquid stream to define the sheet's surface. In the final gas-liquid interaction zone, both fluid channels are confined to a 35 µm x 35 µm cross sectional area. The sample exit is positioned 15 µm downstream of the nozzle outlet.

Nozzle fabrication and assembly

After the print, some steps are needed to clean and cure the photo-resist resin. First, the substrate should be removed and the nozzles must be inserted into a propylene glycol monomethyl ether acetate (PGMEA) solution for around 24 hours. For more complex structures, the beaker should be placed in a shaker to facilitate the revealing process. Afterward, the nozzles should be transferred to 2-propanol to wash away the remaining PGMEA. Finally, after the cleaning, the nozzles need to be placed in a cleanroom at ambient conditions until completely dry.

Silica capillaries a few meters in length and with an outer diameter of 360 µm are used to deliver both the liquid sample and the gas to the nozzle. The process of attaching capillaries to a dry nozzle is described below.

Step 1: The dry nozzle is first fixed onto a PDMS (polydimethylsiloxane) pad using Kapton adhesive tape.

Step 2: The capillaries are cut and marked, usually using a ceramic blade to make the edges as flat as possible. Visual inspection with a microscope is used to ensure this.

Step 3: The capillaries are then glued to the nozzles. We have used two different glues: a five-minute Epoxy and UV-glue Nordland Optical Adhesive 68. For the Epoxy case, the glue was mixed for one minute, and a drop of glue was applied on top of the capillaries and the 3D-printed nozzle to seal them together. It was necessary to wait for the glue to set for at least 10 minutes before moving the assembly. For the UV glue case, we used a UV pencil (Honle UV technology) to cure a drop of glue.

Step 4: Finally, the fixed nozzle was inserted into a stainless steel tube for easy mounting on the nozzle holder, and a new drop of glue was needed on both sides of the tube to help seal the nozzle holder when used under vacuum conditions.

5.3 Commissioning flat jet nozzles

For the initial tests, six nozzles[6] were designed in collaboration with the Sample Environment and Characterization (SEC) and Spectroscopy and Coherent Scattering (SCS) groups from EuXFEL, figure 22. Our goal was to obtain a flat jet sheet bigger than the FlexPES beam spot size (∼300 x 100 µm - HxV) and with a thickness in the micrometer scale, which would give possibilities for XAS measurements in transmission mode using soft X-rays.

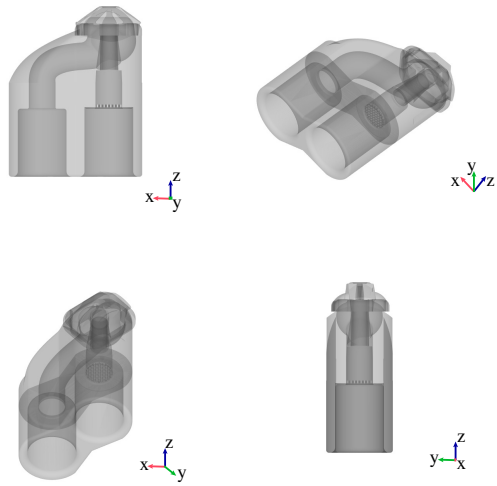

Figure 22: 3D model of the nozzle at various orientation angles, to more clearly demonstrate the design.(**Paper II**)

Following the assembly of the nozzles, all designs were subjected to testing in SEC user laboratories, using the test setup illustrated in Figure 23. The goal of the assessment was to select designs that exhibited stability and alignment when rotated, and to determine their suitability for production and subsequent commissioning at MAX IV.

[6]Only the most successful designs will be showcased.

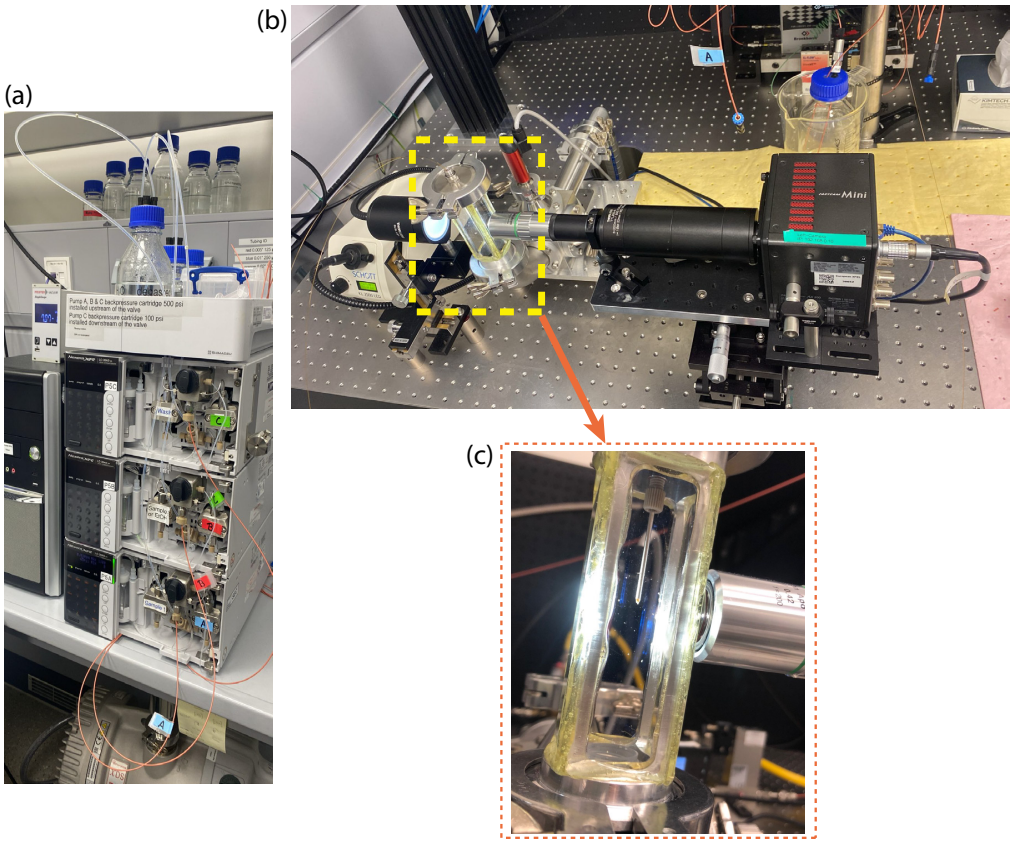

Figure 23: EuXFEL's SEC user laboratory, (a) HPLC pump Nexera XR LC-20AD, (b) Bronkhorst gas flow meter, electronic pressure regulator GP2, and Photon fastcam Mini with 20x objective, and (c) test chamber.

Paper II shows the flat sheet measurements, presented in figure 24, which were obtained in atmosphere using an HPLC pump (Nexera XR LC-20AD for water and ethanol, Cetoni for glycerin), a gas flow meter (Bronkhorst), an electronic pressure regulator (GP2), and a camera (Photon fastcam Mini with 20x objective). As mentioned above, these flat jet nozzles generate a flat jet by converging gas and liquid channels in the collision region, but the behavior varies with different flow rates of liquids and gases, and we have established specific ranges where jet stability can be maintained. The evaluation of nozzle performance also involved experiments with fluids of different viscosities, as described in **Paper III**.

Figure24 illustrates the relationship between the concentration of He in a fixed liquid flow and the stability of the sheet. If the He flow is insufficient, the resulting jet is almost cylindrical; however, if the flow is excessive, a sheet fracture will occur. The same degree of caution is required when considering a fixed He gas flow and a varied liquid flow.

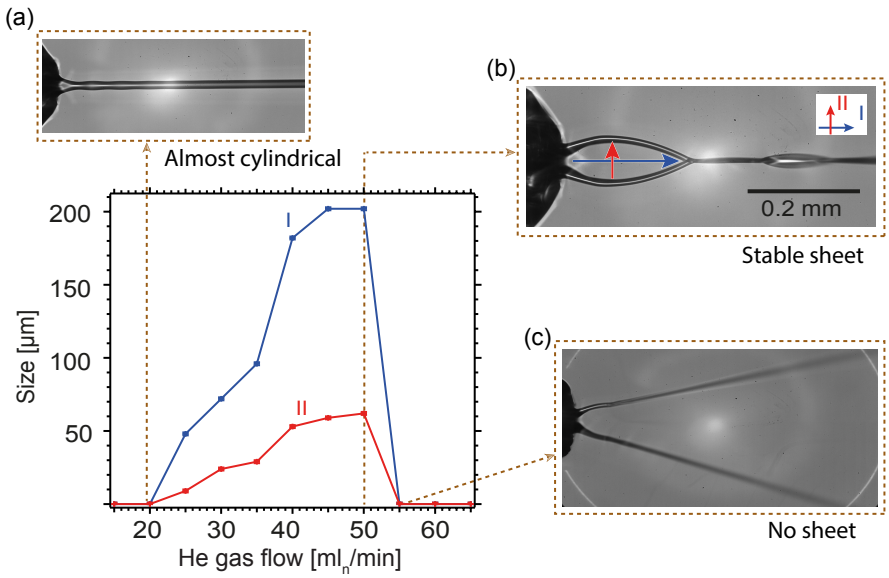

Figure 24: Schematic representation for the He gas and liquid flow to obtain a flat jet surface for pure deionized water. Where the water flow is kept constant at 0.25 ml/min while the He is changed. The relation between both flows can lead to a stable jet in different diameter sizes shown in the graph, where lines (a) and (b) represent the sheet length and width, respectively(**Paper II**).

The performance of the nozzle was also tested using liquids with varying viscosities, including mixtures of ethanol and deionized water with volume ratios of 1:3, 1:1, and 3:1, as well as glycerin and deionized water with ratios of 1:3 and 1:1. In **Paper III**, stability diagrams for water-glycerine and water-ethanol mixtures are presented. Viscosity, the flow resistance of a fluid, has an impact on nozzle performance, and nozzles have practical viscosity limits. When the viscosity of a fluid is high, it can result in reduced spray angle and flow rate, compromising jet formation and stability. Selecting the right nozzle design can reduce this problem, for example, the high-viscosity extruder (HVE), created by Weierstall et al.[98] for high-viscous samples, or a GDVN for faster and smaller jets, improved by Vakili et al.[79]. In addition, temperature can affect viscosity and should be taken into account.

To summarize: The dimensions and stability of a planar liquid sheet, generated by helium gas flow, are influenced by various factors, including liquid viscosity and the flow rates of both liquid and gas. The viscosity of a liquid directly affects nozzle performance as it affects fluid resistance. High viscosity can reduce the spray angle and flow rate, compromising the formation and stability of the liquid sheet.

Based on the experimental data, distinct regions of stability and instability have been identified for different liquid viscosities using both a 3D-printed nozzle and a Micronit chip under atmospheric conditions. An example of a jet stability diagram presented in **Paper III** is shown in Figure 25 for pure water using the 3D-printed nozzle (a) and the Micronit chip (b). The stability diagram, represented by colored areas, indicates conditions in which a stable liquid sheet forms, while white areas indicate unstable regions. To generate large and stable water sheets, higher helium flow rates (60-150 ml$n$/min) are required for the Micronit chip compared to the 3D-printed nozzle (20-50 ml$n$/min). This makes the 3D-printed nozzle advantageous in vacuum environments, due to more stringent vacuum requirements when using soft X-ray detectors. The liquid flow rate range for stable and large planar sheets is wider for the Micronit chip (0.10-0.35 ml/min) compared to the 3D-printed nozzle (0.20-0.40 ml/min) at lower helium flows.

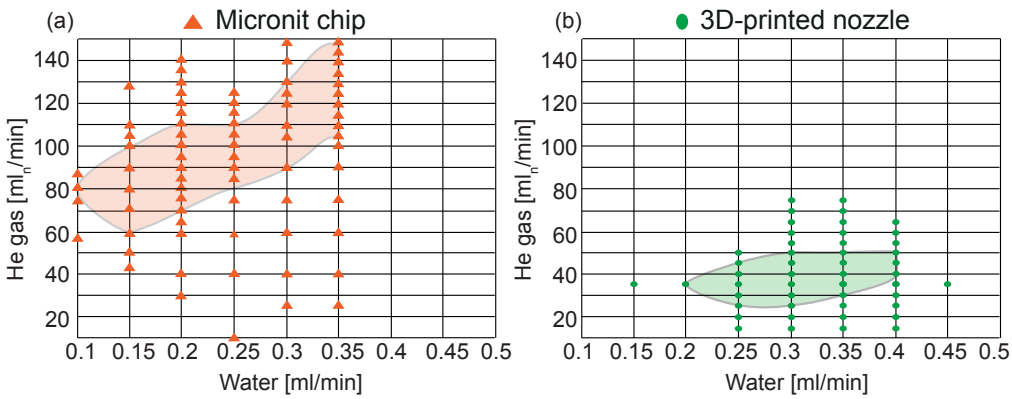

Figure 25: The diagram illustrates the stability of a large flat sheet jets of water (shaded areas), as a function of gas and liquid flow rates. The diagram considers two different nozzle types: (a) a Micronit chip (orange triangle) and (b) a 3D-printed nozzle (green circle) (**Paper III**)

Figure 26 shows the initial dimensions of the liquid sheet produced by both the 3D-printed nozzle (panels a and c) and the Micronit chip (panels b and d) under varying helium and water flow rates. For both nozzle types, the sheet length (panels a and b) and width (panels c and d) increase with increasing helium flow.

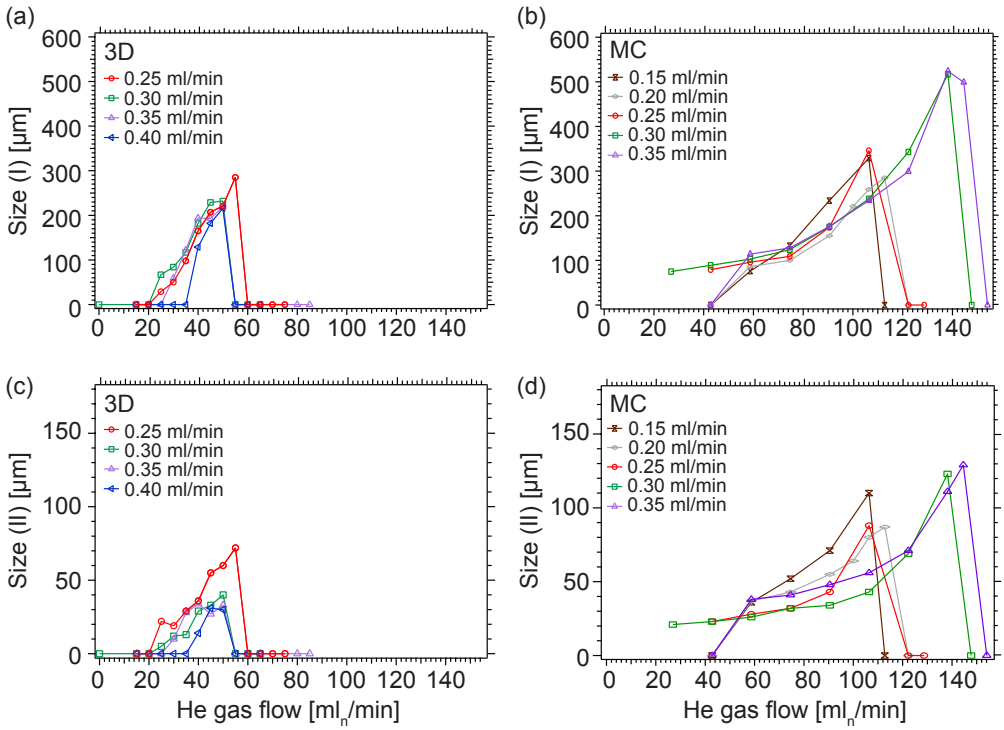

Figure 26: Water flat sheet jet dimensions at different helium and liquid flow rates for the two different nozzles in the study: 3D-printed nozzle (panel (a) and (c)) and micronit chip (panel (b) and (d)). Panels a and b illustrate the jet length and (c) and (d) the jet width (**Paper II** and **Paper III**).

The Micronit chip (panels b and d) requires higher helium flow rates (approximately 100-145 ml$n$/min) compared to the 3D-printed nozzle (approximately 50 ml$n$/min) to achieve maximum sheet size. At a helium flow of 55 ml$_n$ / min, the 3D-printed nozzle produces a sheet of approximately 285 µm by 72 µm, while the Micronit chip forms a smaller sheet of about 96 µm by 28 µm. Increasing the liquid flow for the Micronit chip (to 0.30 and 0.35 ml/min) results in larger sheets of approximately 517 µm by 123 µm and 499 µm by 129 µm, respectively. In contrast, the 3D-printed nozzle (panels a and c) maintains relatively consistent sheet sizes at 0.30, 0.35 and 0.40 ml/min, with these dimensions being smaller than those achieved at 0.25 ml/min.

The optimal conditions for the formation of larger sheets using the 3D-printed nozzle are a water flow of 0.25 ml/min and a helium flow of 55 ml$_n$/min (panels a and c). The Micronit chip requires lower liquid flow rates but higher helium flows to produce stable sheets compared to the 3D-printed nozzle.

Paper III presents the sheet thickness of a flat liquid jet generated by a 3D-printed nozzle under ambient conditions (room temperature of 20-25°C and atmospheric pressure). Just like the jet length and width, the jet thickness is influenced by two main parameters: gas flow and sample flow through the nozzle. The flow rates were adjusted to maintain stability, as shown in the stability diagram (Figure 25). It was observed that the jet thickness decreases with increasing gas flow rates (Figure 27). Stable jets were achieved with gas flow rates between 6-12 mg/min, while lower or higher rates led to instability. At low gas flow rates (6-7 mg/min), adjusting the water flow between 0.15-0.50 ml/min produced jets with thicknesses ranging from 200-4000 nm. Higher gas flow rates (10-11 mg/min) reduced jet thickness to 100-1000 nm. In summary, the offline tests highlight the importance of balancing water and gas flow rates to control stability, size, and jet thickness.

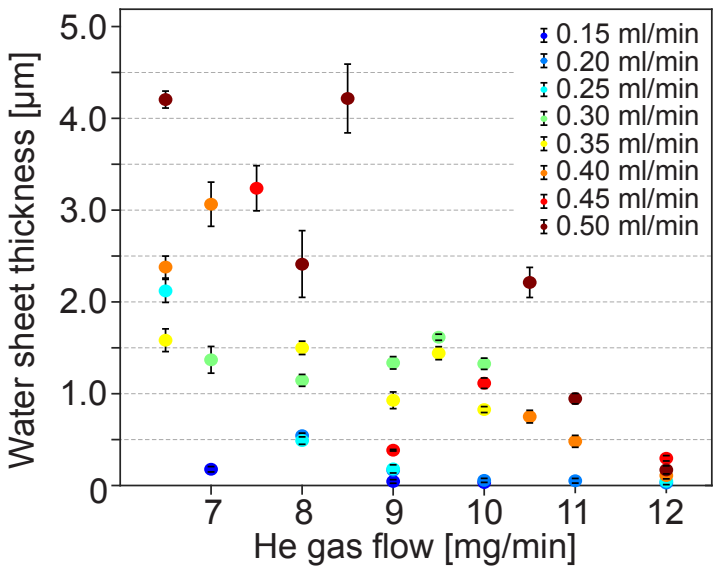

Figure 27: The flat jet thickness for various helium and liquid flow rates. The jet is generated from the 3D-printed nozzle at ambient atmospheric conditions (**Paper III**).

5.4 MAX IV infrastructure for implementing 3D flat jet nozzles

In addition to demonstrating the feasibility of producing a flat jet using aqueous solutions with a large sheet size, we needed to ensure that the flat sheet nozzle could be used in the vacuum environment of the photoemission endstation at FlexPES. The main aim, therefore, was to adapt the holder for the 3D-printed nozzle such that it was compatible with the UHV chamber at FlexPES so that the flat jet could be used with as much of the existing infrastructure as possible for photoelectron and absorption spectroscopy measurements.

The photoemission endstation is equipped with a Scienta R4000 hemispherical photoelectron analyzer. In addition, an AXUV20A photodiode (Opto Diode Corp.) was installed downstream for X-ray absorption measurements, located outside the differentially pumped interaction region of the endstation (Figure 28 a), and this required modifications to the original design of the differential pumping insert. The liquid jet is directed perpendicular to both the photon beam and the spectrometer lens axis during experiments, figure 28b. A custom-designed rod system, which incorporates a modified nozzle holder based on Weierstall's design[55] (Figure 28c), is used for jet injection.

To maintain acceptable vacuum conditions, a liquid nitrogen-cooled trap is installed opposite the liquid jet nozzle (Figure 28a) in the main experimental chamber. This trap effectively removes water vapor from the chamber, and freezes the jet when it hits the cold surface. To prevent the build-up of icicles, that eventually could reach into the interaction region, a rotating "ice breaker" is mounted just in front of the cold trap. The precise alignment of the jet, approximately 1 ± 0.1 mm from the opening of the skimmer cone, and critical for electron detection, is done with an XYZ manipulator. The nozzle rod (Figure 28c) is mounted on a rotary stage, to allow adjustment of the angle of the liquid sheet relative to the incoming radiation.

Further details about the setup and the catcher system that is intended to replace the liquid-nitrogen cooled traps, and which is ready to be commissioned, can be found in the Appendix.

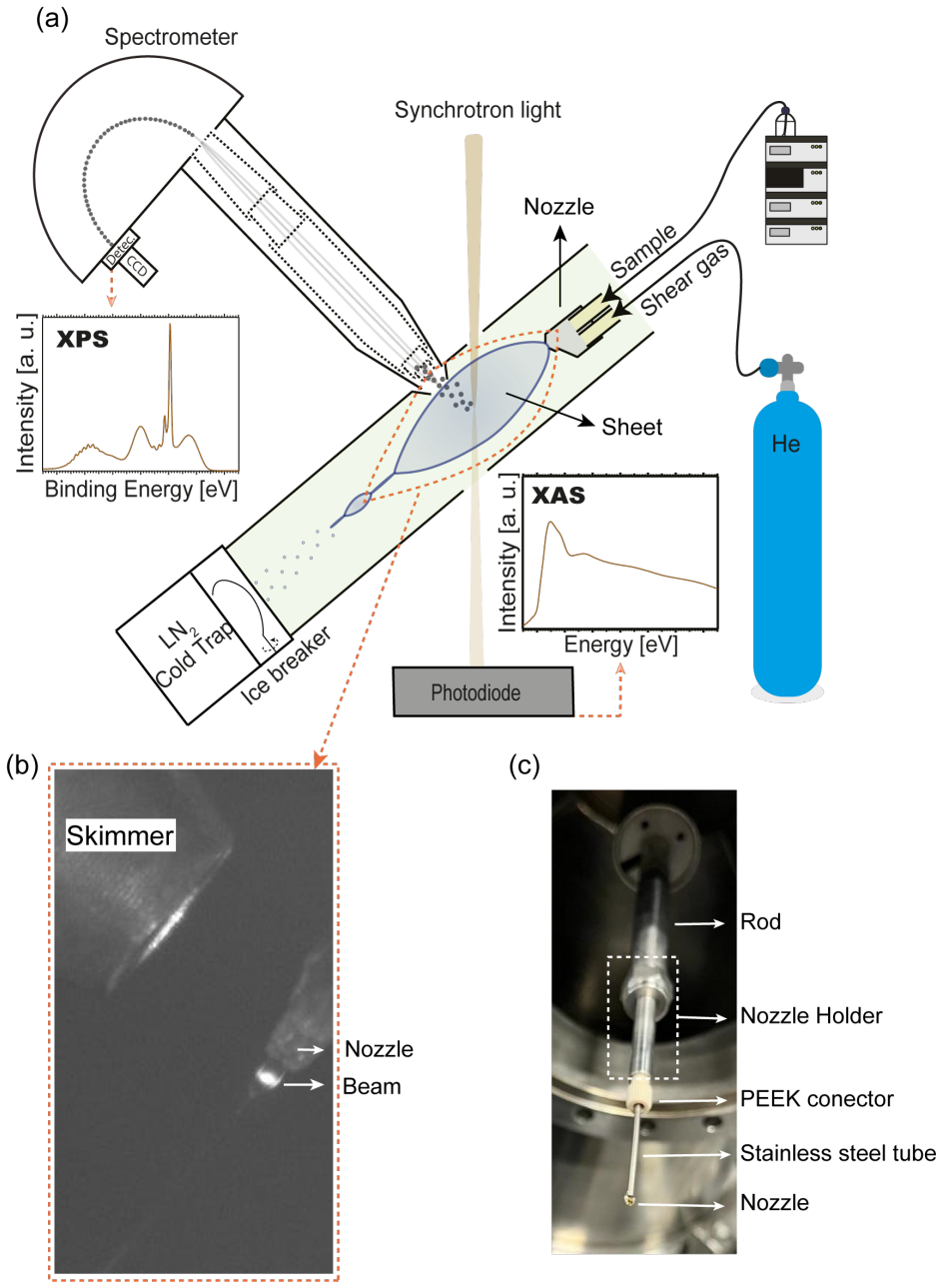

Figure 28: (a) Schematic Diagram: A simplified representation of the liquid jet apparatus is shown, as implemented within the FlexPES beamline's photoemission endstation. Note that this diagram is not proportionally accurate and the nozzle-skimmer distance is exaggerated for visual clarity. b) Experimental Configuration: A close-up view of the experimental setup is presented. A 3D-printed nozzle, positioned at a near-zero takeoff angle, is employed in conjunction with a skimmer featuring a 2 mm aperture. The FlexPES beamline's white beam is directed at a saturated fluorescein solution on a flat surface sample, inducing fluorescence. c) Nozzle Assembly: The standard nozzle holder and essential components for securing the 3D-printed nozzle to the rod are depicted (**Paper II**).

5.5 Application of the flat-jet in real scientific cases

One very appealing quality of flat jets is that by adjusting the angle between the liquid sheet surface and the direction towards the spectrometer, the probing depth in XPS can be varied to investigate surface phenomena. Electrons emitted from a point below the surface will have to travel a longer distance in the liquid for a grazing emission angle than for a normal emission angle. Due to inelastic scattering, the bulk signal will therefore be more suppressed at grazing emission angles. This is showcased in **Paper II**, where an aqueous solution of ethanol and potassium formate is used as a proof-of-principle sample, and it is used to examine the surface propensity of the ammonium and nitrate ions in an aqueous solution of ammonium nitrate, as discussed in **Paper I**.

Paper II demonstrates the feasibility of producing a large flat jet using aqueous solutions after determining the optimal conditions for achieving high stability in the flat sheet produced by 3D-printed nozzles, presented in **Paper III**. As explained above, these nozzles, used for the first time on the FlexPES beamline at MAX IV, produce planar jets that have ∼micrometer thickness, and are large enough to cover the beam spot in focus (figure 28b). This ensures that the flat sheet nozzle is suitable for soft X-ray experiments in a vacuum, and can operate in the vacuum environment of the photoemission endstation at FlexPES.

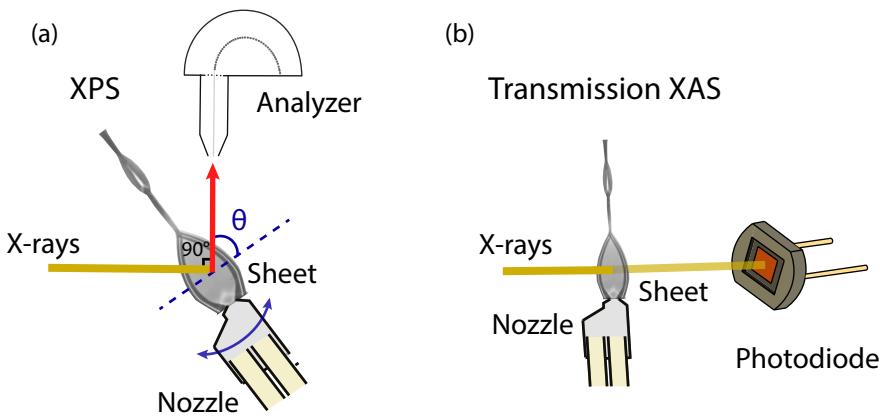

Figure 29: Diagram representation of geometry for (a) XPS and PAD, where the sample take-off angle can be varied by rotating the nozzle relative to the detector, and (b) soft X-ray transmission spectroscopy on a flat surface (**Paper II**).

To examine the composition of the liquid surface using a flat jet, we adjusted the angle at which the electrons are emitted from the surface of the jet toward the spectrometer, the take-off angle, as illustrated in figure 29, using a rotary stage. Practically, the take-off angle is determined by rotating the sheet and observing

at what angle it becomes narrowest (viewed co-linearly with the spectrometer lens axis, defined as 0°) and using the angular scale on the rotary stage to set the desired angle.

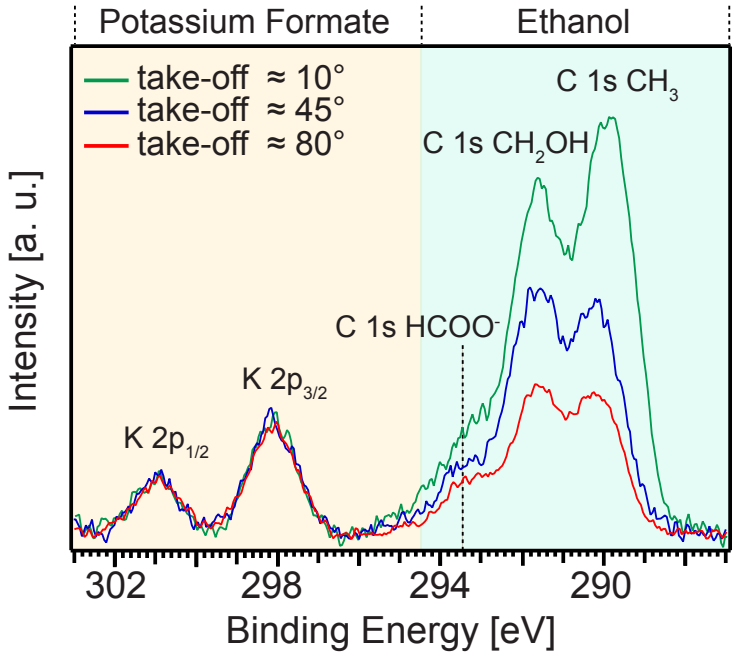

Figure 30: C 1s XP spectra from aqueous solution in 0.2 mol% (0.1 M) ethanol of 0.4 M potassium formate (KHCOO), recorded with three take-off angles from a flat surface produced by a 3D-printed nozzle at 10° (t:10° green), 45° (t:45° blue), and 80° (t:80° red). (**Paper II**)

Figure 30, from **Paper II** shows the C 1s photoelectron spectra of 0.2 mol% (0.1 M) ethanol and 0.4 M potassium formate (KHCOO) in aqueous solution. The spectra were recorded at a photon energy of 360 eV and at the emission angles $\theta = 54.7°$ relative to the horizontally polarized radiation. Data were collected for three take-off angles (relative to the analyzer) from the surface of a flat jet produced by a 3D-printed nozzle at 10° (t:10° green), 45° (t:45° blue), and 80° (t:80° red). All spectra were normalized to the intensity of the K $2p3/_2$ signal, with a polynomial background subtracted.

The potassium ions are expected to avoid the surface region of water[99], whereas ethanol is surface enriched in water[100], and this is clearly shown by the relative increase of the ethanol signal when the take-off angle is decreased towards more grazing angles. The signal intensity as a function of emission angle can in principle be used as a means to find the concentration depth profile in a liquid[101], but the aim of this study was only to show the feasibility of such measurements.

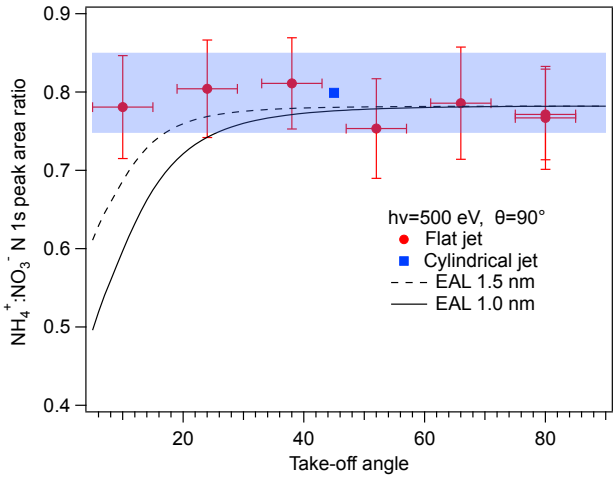

Figure 31: NH_4^+:NO_3^- peak-area ratio obtained from N 1s spectra recorded with a flat jet as a function of take-off angle from 1.0 M NH_4NO_3, as presented in **Paper I**.

In **Paper I** both cylindrical microjets and flat liquid jets were used. The conventional cylindrical nozzles were used to investigate the angular distributions of N 1s photoelectrons relative to the polarization direction of the radiation from ammonium nitrate in aqueous solution, and the flat liquid jet was used to investigate the surface propensity of the ammonium and nitrate ions. These effects are interlinked, since the distance to the surface will also change the probability for elastic scattering, which affects the measured angular distribution. The results of the angular distribution study is summarized in the next chapter, and here only the flat jet measurement will be described.

In Figure 31, the ratio of the (NH_4^+:NO_3^-) N 1s peak areas for a 1.0 M (NH_4NO_3) aqueous solution as a function of the take-off angle is shown. There is no significant dependence on the angle, which indicates a similar distribution of (NH_4^+) and (NO_3^-) ions in the near-surface region. The measured ratio matched well with the value obtained using a cylindrical jet under the same conditions (blue symbol). For this case, we did the opposite to what was mentioned above: Instead of finding the depth distribution from the angle-dependent spectra, which is very complex, we estimated what the angle-dependent intensities would be for a given depth distribution, which is much simpler. Using published data from MD simulations[102], a simple simulation was done to see what intensities would be measured when changing the angle. For small take-off angles, there is a substantial deviation, showing that the MD simulation exaggerates the difference between the ammonium and nitrate concentrations in the surface region.

6 Summary of papers and outlook

In this thesis, I have studied the impact of angular distributions on X-ray photoelectron spectroscopy data from aqueous solutions through two complementary investigations.

In the first study, presented in **Paper I**, I examined the angular distribution of N 1s photoelectrons from a solution of 1.0 M aqueous ammonium nitrate, with spectra acquired at 54.7° and 90°, and photon energies ranging from 470 to 530 eV. This study investigated factors that affect the angular anisotropy of photoelectrons, quantified through values of β, and assessed the surface propensity of ions ($NH_4{}^+$) and ($NO_3{}^-$). I investigated the influence of measurement geometry on X-ray photoelectron spectroscopy data from liquid phase samples, using two types of liquid jet nozzle: a cylindrical microjet and a flat jet, to measure the N 1s photoelectrons at different angles and photon energies.

The photoelctron angular anisotropy data was obtained using a cylindrical nozzle. By comparing the ammonium and nitrate peak area ratios acquired for both angles, I discussed possible conclusions about the propensity of the ions for the surface. Auxiliary measurements using a flat jet nozzle found that the ammonium and nitrate peak area ratio was not affected by changes in the take-off angle, indicating a similar distribution of ammonium and nitrate in the surface region. Finally, β values were obtained as a function of the photon energy, using a normalization procedure based on simulations of the background intensity with the SESSA package[56]. In the simulations, the take-off angle from the cylindrical surface of the jet was modeled using a range of planar surfaces, since SESSA does not offer the possibility of simulations involving a cylindrical surface. The angle between the planar surface of the sample and the spectrometer was varied from 0° to 100° in steps of 5°. To investigate the possible influence of variations in the surface concentration of the solute in the microjet, a three-layer description of the sample was used. The upper layer was 2 Å thick and contained water molecules. The second layer was 5 Å thick and contained varying amounts of NH_4NO_3. The spectral difference in the region of interest for the applied simulation parameters for these sample variations is quite small. Therefore, the simulations show that possible density variations in the surface region will have only a small influence on the results for the background (region of interest).

The β value for N 1s from NH_4^+ was found to be slightly higher than that for NO_3^- over the entire photon energy range investigated. Together with the observation from the flat jet measurement that the ammonium and nitrate ions have similar

depth distributions, we could conclude that this difference is due to inherent properties of the ions. Additionally, the photoelectron signal from nitrate exhibited a photon energy-dependent cross-section variation, a phenomenon not observed for ammonium, suggesting that intra-molecular scattering processes strongly influence the photoelectron emission from the nitrate ion.

The second study, presented in **Paper IV**, focuses on potassium carboxylate solutions, including potassium acetate, formate, propanoate, butanoate, and hexanoate, at concentrations ranging from 0.025 M to 1 M. Using a cylindrical liquid jet setup, I collected XP spectra at emission angles of 54.7° and 90° relative to the synchrotron radiation polarization, with photon energies from 360 to 550 eV. This study shows how molecular structure, particularly the length of the alkyl chain, influences the molecular orientation and surface propensity, which in turn has an effect on the measured angular distribution. The photoelectron angular distributions (PADs) are found to be differently influenced by elastic scattering when going from bulk solvated to strongly surface-active species, and this study provides insight into the relative depth and location of the carboxylate functional groups, illustrating that this is a valuable method for investigating the adsorption of organic molecules at liquid-vapor interfaces.

These studies jointly show that angular effects influence the XP spectra when studying both the electronic and surface properties of solutes in aqueous solutions, highlighting the critical importance of considering angular distribution effects when interpreting XPS data from liquid-phase systems. The liquid microjet technique, combined with the measurement of PADs, presents a promising avenue for determining the electronic and surface properties of solutes in liquid water and at the liquid-vapor interface.

To overcome the limitations of traditional cylindrical microjets for liquid spectroscopy studies, I collaborated with EuXFEL groups to develop a novel 3D-printed flat sheet nozzle custom-designed for implementation at the FlexPES beamline. This design offers enhanced stability, increased surface area, and compatibility with various experimental techniques, including XPS, photoelectron angular distribution studies, and soft X-ray absorption spectroscopy.

Paper II introduces a 3D-printed flat sheet nozzle that generates microscopic flat sheet jets for soft X-ray spectroscopy. Its performance is demonstrated using XPS and XAS experiments, which shows that the nozzle delivers stable and thin liquid sheets suitable for various X-ray analysis methods. The flat sheet nozzle, implemented for the first time on the FlexPES beamline at MAX IV, produces planar jets of the order of micrometers in thickness, that are large enough to cover the beam spot in focus, and which are stable at low sample and

gas flow rates. This ensures acceptable vacuum conditions in the main chamber of photoemission endstation at the FlexPES beamline.

We studied C 1s photoelectrons from an aqueous solution containing 0.2 mol% ethanol and 0.4 M potassium formate. Using the flat sheet jet produced by our 3D-printed nozzle and a new jetting platform, we recorded spectra at various take-off angles (presented in Fig. 30), demonstrating the effectiveness of the developed injection system in generating large, stable, and uniform sheets, which leads to high surface yield. We also recorded transmission XAS data for an aqueous solution of ammonium nitrate in the vicinity of the N 1s edge, showing the feasibility of performing XAS measurements with the new flat jet design.

Paper III demonstrates the performance and gives a detailed characterization of the flat sheet jets produced by both a 3D-printed nozzle and the commercial microfluidic chip from Micronit. The use of 3D-printed nozzles allow for quick prototyping and iterative design optimization, enhancing the efficiency and overall performance of the nozzle system. Our results show that 3D-printing technology offers a powerful and flexible tool for creating flat sheet jet nozzles for soft X-ray spectroscopy and other applications.

We compared the 3D-printed nozzle with the commercial chip from Micronit. Both produced sheets thin enough for soft X-ray experiments, but the 3D-printed nozzle created sheets that were 2-4 µm thick, with better stability and lower consumption of helium and liquid flow compared to the Micronit chip. This makes the 3D-printed nozzle more suitable to achieve acceptable vacuum conditions when working with X-ray detectors, such as the electron spectrometer MCP detector of the photoemission endstation at the FlexPES beamline. The sheet size was sufficient to cover the beam spot at FlexPES, and the nozzle operated well under vacuum conditions, allowing us to perform XPS and XAS experiments.

Moreover, a detailed stability study on the dimensions and thickness of the flat sheet jets was conducted for liquids with different viscosities and concentrations, using samples such as ethanol: water, glycerin: water, and isopropanol. The flat sheet jets formed by ethanol have a smaller stability range than those obtained with water. In addition, the size of the planar sheets is inversely related to the viscosity of the liquid. This means that for fluids with higher viscosity it is more difficult to produce large sheets at the same flow rate, while a lower viscosity results in larger sheet sizes. The higher viscosity also offers more flexibility in maintaining a stable sheet with varying helium-gas flow.

This thesis demonstrates the potential of the 3D-printed flat-sheet nozzle for advancing liquid-phase soft X-ray spectroscopy studies. The nozzle developed

as a part of this work has been shown to fulfill the requirements for operation at the FlexPES beamline, facilitating transmission-mode XAS measurements and XPS, where the ability to change the electron emission angle by rotating the liquid sheet opens up for a wealth of new experiments in the field of liquid-phase photoelectron spectroscopy. The use of these new flat sheet nozzles in X-ray spectroscopic methods can provide valuable insights into the electronic and surface properties of solutes in liquid water and at the liquid-vapor interface, with potential applications in atmospheric chemistry, biophysics, and materials science. Future research directions envisaged as a follow-up to this work would explore the use of a similar flat sheet nozzle design for other X-ray analysis methods at MAX IV, for example liquid-phase RIXS. The Veritas beamline have performed some initial tests with a commercial flat sheet nozzle and observed a gain in intensity when using a flat sheet for RIXS measurements compared to experiments with a cylindrical jet. A custom-designed flat liquid sheet of few micrometer thickness which is optimised for RIXS experiments at the beamline could help to further minimize self-absorption whilst also improving vacuum conditions under jet operation.

7 References

[1] J. James. *Spectrograph Design Fundamentals.* Cambridge University Press, 2007.

[2] Donald L. Pavia, Gary M. Lampman, and George S. Kriz. *Introduction to Spectroscopy.* Cengage Learning, 5th edition, 2014.

[3] M. Faubel, B. Steiner, and J. P. Toennies. Photoelectron spectroscopy of liquid water, some alcohols, and pure nonane in free micro jets. *J. Chem. Phys.*, 106(21):9013–9031, 1997.

[4] N. L. Prisle, N. Ottosson, G. Öhrwall, J. Söderström, M. Dal Maso, and O. Björneholm. Surface/bulk partitioning and acid/base speciation of aqueous decanoate: Direct observations and atmospheric implications. *Atmos. Chem. Phys.*, 12(24):12227–12242, 2012.

[5] H. Morgner. The investigation of liquid surfaces by electron spectroscopy. *J. Electron Spectrosc. Relat. Phenom.*, 68:771–777, 1994.

[6] B. Winter. Liquid microjet for photoelectron spectroscopy. *Nucl. Instrum. Methods Phys. Res., Sect. A*, 601(1–2):139–150, 2009.

[7] H. Siegbahn and K. Siegbahn. ESCA applied to liquids. *J. Electron Spectrosc. Relat. Phenom.*, 2(3):319–325, 1973.

[8] H. Siegbahn, L. Asplund, P. Kelfve, K. Hamrin, L. Karlsson, and K. Siegbahn. ESCA applied to liquids. II. Valence and core electron spectra of formamide. *J. Electron Spectrosc. Relat. Phenom.*, 5(1):1059–1079, 1974.

[9] H. Fellner-Feldegg, H. Siegbahn, L. Asplund, P. Kelfve, and K. Siegbahn. ESCA applied to liquids IV. A wire system for ESCA measurements on liquids. *J. Electron Spectrosc. Relat. Phenom.*, 7(5):421–428, 1975.

[10] H. Siegbahn. Electron spectroscopy for chemical analysis of liquids and solutions. *J. Phys. Chem.*, 89(6):897–909, 1985.

[11] M. Faubel, S. Schlemmer, and J. P. Toennies. A molecular beam study of the evaporation of water from a liquid jet. *Z. Physik D: At., Mol. Clusters*, 10:269–277, 1988.

[12] Z. Wu, Z. Jiang, W. Yan, Y. Yang, J. Kang, K. Zheng, W. Bu, W. Wang, and B. Song. Jet microchannel with sawtooth wall for efficient cooling of high-power electronics. *Int. J. Heat Mass Transfer*, 206:123955, 2023.

[13] D. L. Muccignat, P. W. Stokes, D. G. Cocks, J. R. Gascooke, D. B. Jones, M. J. Brunger, and R. D. White. Simulating the feasibility of using liquid micro-jets for determining electron–liquid scattering cross-sections. *Int. J. Mol. Sci.*, 23(6):3354, 2022.

[14] M. Vakili, R. Vasireddi, P. V. Gwozdz, D. C. F. Monteiro, M. Heymann, R. H. Blick, and M. Trebbin. Microfluidic polyimide gas dynamic virtual nozzles for serial crystallography. *Rev. Sci. Instrum.*, 91(8):085108, 2020.

[15] Z. Faraji Rad, P. D. Prewett, and G. J. Davies. High-resolution two-photon polymerization: The most versatile technique for the fabrication of microneedle arrays. *Microsystems & Nanoengineering*, 7(1):71, 2021.

[16] T Lewis, M. Faubel, B. Winter, and J. C Hemminger. CO_2 capture in amine-based aqueous solution: Role of the gas–solution interface. *Angew. Chem. Int. Ed.*, 50(43):10178–10181, 2011.

[17] E. Vanea and V. Simon. XPS study of protein adsorption onto nanocrystalline aluminosilicate microparticles. *Appl. Surf. Sci.*, 257(6):2346–2352, 2011.

[18] N. Ottosson, K. J. Børve, D. Spångberg, H. Bergersen, L. J. Sæthre, M. Faubel, W. Pokapanich, G. Öhrwall, O. Björneholm, and B. Winter. On the origins of core-electron chemical shifts of small biomolecules in aqueous solution: Insights from photoemission and ab initio calculations of glycine(aq). *J. Am. Chem. Soc.*, 133(21):807–811, 2011.

[19] P. Scodeller, F. J. Williams, and E. J. Calvo. XPS analysis of enzyme and mediator at the surface of a layer-by-layer self-assembled wired enzyme electrode. *Anal. Chem.*, 86(24):12180–12184, 2014.

[20] Á. Silva, A. Mocellin, S. Monti, C. Li, R. R. Marinho, A. Medina, H. Ågren, V. Carravetta, and A. N. de Brito. Surface-altered protonation studied by photoelectron spectroscopy and reactive dynamics simulations. *J. Phys. Chem. Lett.*, 6(5):807–811, 2015.

[21] O. Björneholm, G. Öhrwall, A. N. de Brito, H. Ågren, and V. Carravetta. Superficial tale of two functional groups: On the surface propensity of aqueous carboxylic acids, alkyl amines, and amino acids. *Acc. Chem. Res.*, 55(23), 2022.

[22] D. Chivian, E. L. Brodie, E. J. Alm, D. E. Culley, P. S. Dehal, T. Z. DeSantis, T. M. Gihring, A. Lapidus, L.-H. Lin, and S. R. Lowry. Environmental genomics reveals a single-species ecosystem deep within Earth. *Science*, 322(5899):275–278, 2008.

[23] C. P. McKay. The search for life on Mars. *Am. Sci.*, 92(4):342–349, 2004.

[24] M. A. Brown, M. Faubel, and B. Winter. X-Ray photo- and resonant Auger-electron spectroscopy studies of liquid water and aqueous solutions. *Annu. Rep. Prog. Chem. Sect. C: Phys. Chem.*, 105(0):174–212, 2009.

[25] D. Chandler. Interfaces and the driving force of hydrophobic assembly. *Nat.*, 437(7059):640–647, 2005.

[26] P. Jungwirth and D. J. Tobias. Specific ion effects at the air/water interface. *Chem. Rev.*, 106(4):1259–1281, 2006.

[27] R. Signorell and B. Winter. Photoionization of the aqueous phase: Clusters, droplets and liquid jets. *Phys. Chem. Chem. Phys.*, 24:13438–13460, 2022.

[28] M. F. Ruiz-Lopez, Joseph S Francisco, Marilia TC Martins-Costa, and Josep M Anglada. Molecular reactions at aqueous interfaces. *Nat. Rev. Chem.*, 4(8):459–475, 2020.

[29] G. M. Kontogeorgis, A. Holster, N. Kottaki, E. Tsochantaris, F. Topsøe, J. Poulsen, M. Bache, X. Liang, N. S. Blom, and J. Kronholm. Water structure, properties and some applications – A review. *Chemical Thermodynamics and Thermal Analysis*, 6:100053, 2022.

[30] J.-P. Hansen and I. R. McDonald. Theory of simple liquids. *Phys. Rev. Lett.*, 97(11):115702, 2006.

[31] J. N. Israelachvili. *Intermolecular and Surface Forces*. Academic Press, Elsevier Inc, 3rd edition, 2011.

[32] Theodore L. Brown, H. Eugene LeMay, and Bruce E. Bursten. *Chemistry: The Central Science*. Pearson, 14th edition, 2017.

[33] Gary L. Miessler, Paul J. Fischer, and Donald A. Tarr. *Inorganic Chemistry*. Pearson, 5th edition, 2013.

[34] W. M. Latimer and W. H. Rodebush. Polarity and ionization from the standpoint of the Lewis theory of valence. *J. Am. Chem. Soc.*, 42(9): 1419–1433, 1920.

[35] R. V'acha, O. Marsalek, A. P. Willard, D. J. Bonthuis, R. R. Netz, and P. Jungwirth. Charge transfer between water molecules as the possible origin of the observed charging at the surface of pure water. *J. Phys. Chem. Lett.*, 3(1):107–111, 2012.

[36] E. Arunan. One hundred years after the Latimer and Rodebush paper, hydrogen bonding remains an elephant! *J. Indian Inst. Sci.*, 100(3):249–255, 2020.

[37] P. Ball. *The Hydrogen Bond and the Water Molecule: The Physics and Chemistry of Water, Aqueous and Bio Media.* Elsevier Science, 2007.

[38] E. Aziz, N. Ottosson, M. Faubel, I. V. Hertel, and B. Winter. Interaction between liquid water and hydroxide revealed by core-hole de-excitation. *Nature*, 455:89–91, 2008.

[39] C. Boyars. Reducing the explosion sensitivity of ammonium nitrate fertilizer. *Ind. Eng. Chem. Prod. Res. Dev.*, 15(4):308–309, 1976.

[40] N. Ottosson, J. Heyda, E. Wernersson, W. Pokapanich, S. Svensson, B. Winter, G. Öhrwall, P. Jungwirth, and O. Björneholm. The influence of concentration on the molecular surface structure of simple and mixed aqueous electrolytes. *Phys. Chem. Chem.*, 12:10693–10700, 2010.

[41] N. Ottosson, L. Cwiklik, J. Söderström, O. Björneholm, G. Öhrwall, and P. Jungwirth. Increased propensity of I^-_{aq} for the water surface in non-neutral solutions: Implications for the interfacial behavior of $H_3O^+_{aq}$ and OH^-_{aq}. *J. Phys. Chem. Lett.*, 2(9):972–976, 2011.

[42] G. Öhrwall, N. L. Prisle, N. Ottosson, J. Werner, V. Ekholm, M.-M. Walz, and O. Björneholm. Acid–base speciation of carboxylate ions in the surface region of aqueous solutions in the presence of ammonium and aminium ions. *J. Phys. Chem. B*, 119(10):4033–4040, 2015.

[43] G. Hähner. Near edge X-ray absoption fine structure spectroscopy as a tool to probe electronic and structural properties of thin organic films and liquids. *Chem. Soc. Rev.*, 35:1244–1255, 2006.

[44] N. Smith. Science with soft X-rays. *Phys. Today*, 54(1):29–34, 2001.

[45] J. Eggers and E. Villermaux. Physics of liquid jets. *Rep. Prog. Phys.*, 71 (3):036601, 2008.

[46] E Mariotte. *Traite du mouvement des eaux et des autres corps fluides.* P. E. Michallet (Ed.), 1686.

[47] F. Savart. Mémoire sur la constitution des veines liquids lancees par des orifices circulaires en mince paroi. *Ann.Chim.*, 53:337–386, 1833.

[48] F.R.S. Rayleigh. The instability of jets. *Proc. Lond. Math. Soc.)*, 1(10), 1878.

[49] G. Galinis, J. Strucka, J. C. T. Barnard, A. Braun, R. A. Smith, and J. P. Marangos. Micrometer-thickness liquid sheet jets flowing in vacuum featured. *Rev. Sci. Instrum.*, 88(8):083117, 2017.

[50] M. Ekimova, W. Quevedo, M. Faubel, P. Wernet, and E. T. J. Nibbering. A liquid flatjet system for solution phase soft X-ray spectroscopy. *Struct. Dyn.*, 2(5):054301, 2015.

[51] J. Knoška, L. Adriano, S. Awel, K. R. Beyerlein, O. Yefanov, D. Oberthuer, G. E. Peña Murillo, N. Roth, I. Sarrou, P. Villanueva-Perez, M. O. Wiedorn, F. Wilde, S. Bajt, H. N. Chapman, and M. Heymann. Ultracompact 3D microfluidics for time-resolved structural biology. *Nat. Comm.*, 11(657), 2020.

[52] M. Fondell, S. Eckert, R. M. Jay, C. Weniger, W. Quevedo, J. Niskanen, B. Kennedy, F. Sorgenfrei, D. Schick, E. Giangrisostomi, R. Ovsyannikov, K. Adamczyk, N. Huse, P. Wernet, R. Mitzner, and A. Föhlisch. Time-resolved soft X-ray absorption spectroscopy in transmission mode on liquids at MHz repetition rates. *Struct. Dyn.*, 106:054902, 2017.

[53] J. D. Koralek, J. B. Kim, P. Brůža, C. B. Curry, Z. Chen, H. A. Bechtel, A. A. Cordones, P. Sperling, S. Toleikis, J. F. Kern, S. P. Moeller, S. H. Glenzer, and D. P. DePonte. Generation and characterization of ultrathin free-flowing liquid sheets. *Nat. Comm.*, 9, 2018.

[54] J. F. Lutsko, Q. Zhang, H. Gao, A. Mozzanica, J. S. Pedersen, Y. Wang, M. Lo Russo, M. Guizar-Sicairos, H. Gimenez, C. Grünzweig, R. Spolenak, H. Jiang, and J. Miao. Shear-coaxial liquid sheets for in situ structural studies with X-rays. *Nat. Comm.*, 12(1):1–11, 2021.

[55] U. Weierstall, D. James, C. Wang, T. A. White, D. Wang, W. Liu, J. C. H. Spence, R. B. Doak, G. Nelson, P. Fromme, R. Fromme, I. Grotjohann, C. Kupitz, N. A. Zatsepin, H. Liu, S. Basu, D. Wacker, G. W. Han, V. Katritch, S. Boutet, M. Messerschmidt, G. J. Williams, J. E. Koglin, M. M. Seibert, M. Klinker, C. Gati, R. L. Shoeman, A. Barty, H. N. Chapman, R. A. Kirian, K. R. Beyerlein, R. C. Stevens, D. Li, S. T. A. Shah, N. Howe, M. Caffrey, and V. Cherezov. Lipidic cubic phase injector facilitates membrane protein serial femtosecond crystallography. *Nat. Comm.*, 5:3309, 2014.

[56] W. S. M. Werner, W. Smekal, and C. J. Powell. Simulation of electron spectra for surface analysis (SESSA), version 2.2. Technical report, National Institute of Standard and Technology, Gaithersburg, MD, 2021.

[57] M. Pugini, F. Trinter, I. Wilkinson, B. Credido, I. Walter, D. Stemer, U. Hergenhahn, G. Meijer, B. Winter, and S. Thürmer. How to measure work functions from aqueous solutions. *Chem. Sci.*, 14:9574–9588, 2023.

[58] J. Cooper and R. N. Zare. Angular distribution of photoelectrons. *J. Chem. Phys.*, 48:942–943, 1968.

[59] D. Dill. Fixed-molecule photoelectron angular distributions. *J. Chem. Phys.*, 65:1130–1133, 1976.

[60] R. Dupuy, J. Filser, C. Richter, T. Buttersack, F. Trinter, S. Gholami, R. Seidel, C. Nicolas, J. Bozek, D. Egger, H. Oberhofer, S. Thürmer, U. Hergenhahn, K. Reuter, B. Winter, and H. Bluhm. Ångstrom-depth resolution with chemical specificity at the liquid-vapor interface. *Phys. Rev. Lett.*, 130(15):156901, 2023.

[61] N. Ottosson, M. Faubel, S. E. Bradforth, P. Jungwirth, and B. Winter. Photoelectron spectroscopy of liquid water and aqueous solution: Electron effective attenuation lengths and emission-angle anisotropy. *J. Electron Spectrosc. Relat. Phenom.*, 177:60–70, 2010.

[62] S. Thürmer, R. Seidel, M. Faubel, W. Eberhardt, J. C. Hemminger, S. E. Bradforth, and B. Winter. Photoelectron angular distributions from liquid water: Effects of electron scattering. *Phys. Rev. Lett.*, 111, 2013.

[63] Y.-I. Suzuki, K. Nishizawa, N. Kurahashi, and T. Suzuki. Effective attenuation length of an electron in liquid water between 10 and 600 eV. *Phys. Rev. E*, 90:010302, 2014.

[64] R. Signorell. Electron scattering in liquid water and amorphous ice: A striking resemblance. *Phys. Rev. Lett.*, 124:205501, 2020.

[65] G. A. Somorjai. *Chemistry in Two Dimensions: Surfaces.* Cornell University Press, Ithaca, NY, 1981.

[66] H. Shinotsuka, B. Da, S. Tanuma, H. Yoshikawa, C. J. Powell, and D. R. Penn. Calculations of electron inelastic mean free paths XI. Data for liquid water for energies from 50 eV to 30 keV. *Surf. Interface Anal.*, 49 (4):238–252, 2017.

[67] J. Stöhr. *NEXAFS spectroscopy.* Springer-Verlag Berlin Heidelberg, 1992.

[68] I. A. Vartanyants and A Singer. Coherence properties of third-generation synchrotron sources and free-electron lasers. In Erik Jaeschke, Shaukat Khan, J. R. Schneider, and John B. Hastings, editors, *Synchrotron Light Sources and Free-Electron Lasers*, pages 821–849. Springer, Cham, 2015.

[69] A. Barbier, C. Mocuta, and R. Belkhou. Selected synchrotron radiation techniques. In B. Bhushan, editor, *Encyclopedia of Nanotechnology*. Springer, Dordrecht, 2012.

[70] A. Robert, Y. Cerenius, P. F. Tavares, A. Hultin Stigenberg, O. Karis, A.-C. Lloyd Whelan, C. Runéus, and M. Thunnissen. MAX IV Laboratory. *Eur. Phys. J. Plus*, 138(6):495, 2023.

[71] V. Simoulin. The synchrotron generations communities and facilities at the crossroads between the national and the international. *Revue française de sociologie*, 57(3):340–361, 2016.

[72] V. A. Shkaruba, A. V. Bragin, A. A. Volkov, A. I. Erokhin, A. V. Zorin, F. P. Kazantsev, P. V. Kanonik, N. A. Mezentsev, A. N. Safronov, A. A. Sedov, O. A. Tarasenko, S. V. Khrushchev, and V. M. Tsukanov. Superconducting wigglers and undulators for synchrotron radiation generation at the SKIF storage ring. *Phys. Part. Nuclei Lett.*, 20:904–908, 2023.

[73] A. Preobrajenski, A. Generalov, G. Öhrwall, M. Tchaplyguine, H. Tarawneh, S. Appelfeller, E. Frampton, and N. Walsh. FlexPES: a versatile soft X-ray beamline at MAX IV Laboratory. *J. Synchrotron Radiat.*, 30:831–840, 2023.

[74] George Major, Vincent Fernandez, Neal Fairley, and Matthew Linford. A detailed view of the gaussian–lorentzian sum and product functions and their comparison with the voigt function. *Surface and Interface Analysis*, 54(5):456–467, 2022.

[75] E. Kukk. Spectrum analysis by curve fitting (SPANCF) - macro package for Igor Pro. Technical report, University of Turku, 2012. edwin.kukk@utu.fi.

[76] J. L. Campbell and T. Papp. Widths of the atomic K-N7 levels. *At. Data Nucl. Data Tables*, 77:1–56, 2001.

[77] S. Menzi, G Knopp, A. Haddad, S. Augustin, C. Borca, D. Gashi, T. Huthwelker, D. James, J. Jin, G. Pamfilidis, K. Schnorr, Z. Sun, R. Wetter, Q. Zhang, and C. Cirelli. Generation and simple characterization of flat, liquid jets. *Rev. Sci. Instrum.*, 91:105109, 2020.

[78] M. Vakili, H. Han, C. Schmidt, A. Wrona, M. Kloos, I. de Diego, K. Dörner, J. Valerio, E. Round, K. Lorenzen, and J. Schulz. Mix-and-extrude using 3D printed nozzles for time-resolved membrane protein crystallography. *bioRxiv*, page 2022.11.23.517685, 2022.

[79] M. Vakili, J. Bielecki, J. Knoska, F. Otte, H. Han, M. Kloos, R. Schubert, E. Delmas, G. Mills, R. de Wijn, R. Letrun, S. Dold, R. Bean, A. Round, Y. Kim, F. A. Lima, K. Dörner, J. Valerio, M. Heymann, A. P. Mancuso, and J. Schulz. 3D printed devices and infrastructure for liquid sample delivery at the european XFEL. *J. Synchrotron Radiat.*, 29(2):331–346, 2022.

[80] Y. Chang, Z. Yin, T. Balciunas, H. J. Worner, and J. Wolf. Temperature measurements of liquid flat jets in vacuum. *Struct. Dyn.*, 9:014901, 2022.

[81] R. Dupuy, C. Richter, B. Winter, G. Meijer, R. Schlögl, and H. Bluhm. Core level photoelectron spectroscopy of heterogeneous reactions at liquid–vapor interfaces: Current status, challenges, and prospects. *J. Chem. Phys.*, 154(6):060901, 2021.

[82] A. Stelson, D. Laage, K. Schwarz, and R. Sundararaman. Solid-liquid interfaces: Atomic-scale structure and dynamics. *J. Appl. Phys.*, 135(16): 160401, 2024.

[83] P. S. Pershan and M. Schlossman. *Liquid Surfaces and Interfaces: Synchrotron X-ray Methods*. Cambridge University Press, 2012.

[84] T. Buttersack, H Haak, H. Bluhm, U. Hergenhahn, G. Meijer, and B. Winter. Imaging temperature and thickness of thin planar liquid water jets in vacuum. *Struct. Dyn.*, 10:034901, 2023.

[85] D. Stemer, T Buttersack, H. Haak, S. Malerz, H. C. Schewe, F. Trinter, K. Mudryk, M. Pugini, B. Credidio, R. Seidel, U. Hergenhahn, G. Meijer, S. Thürmer, and B. Winter. Photoelectron spectroscopy from a liquid flatjet. *J Chem. Phys.*, 158(23):234202, 2023.

[86] A. Watanabe, H. Saito, Y. Ishida, M. Nakamoto, and T. Yajima. A new nozzle producing ultrathin liquid sheets for femtosecond pulse dye lasers. *Opt. Comm.*, 71(5):301–304, 1989.

[87] A. M. Gañán-Calvo, D. P. DePonte, M. A. Herrada, J. C. H. Spence, U. Weierstall, and R. B. Doak. Liquid capillary micro/nanojets in free-jet expansion. *Small*, 6:822–824, 2010.

[88] J Klebniczki, J Hebling, B Hopp, G Hajos, and Z Bor. Fluid jet with variable thickness in the range 5-20 μm. *Appl. Phys. B*, 102(4):791–796, 2011.

[89] I. Steinke, M. Walther, F. Lehmkühler, P. Wochner, J. Valerio, R. Mager, M. A. Schroer, S. Lee, W. Roseker, A. Jain, M. Sikorski, S. Song, R. Hartmann, M. Huth, L. Strüder, M. Sprung, A. Robert, P. H. Fuoss, G. B. Stephenson, and G. Grübel. A liquid jet setup for X-ray scattering experiments on complex liquids at free-electron laser sources. *Rev. Sci. Instrum.*, 87:063905, 2016.

[90] G. Galinis, J. Strucka, J. C. T. Barnard, A. Braun, R. A. Smith, and J. P. Marangos. Micrometer-thickness liquid sheet jets flowing in vacuum. *Rev. Sci. Instrum.*, 88:083117, 2017.

[91] C. Kleine, M. Ekimova, G. Goldsztejn, S. Raabe, C. Strüber, J. Ludwig, S. Yarlagadda, S. Eisebitt, M. J. J. Vrakking, T. Elsaesser, E. T. J. Nibbering, and A. Rouzée. Soft X-ray absorption spectroscopy of aqueous solutions using a table-top femtosecond soft X-ray source. *J. Phys. Chem. Lett.*, 9(24):7114–7119, 2018.

[92] D. P. DePonte, U. Weierstall, K. Schmidt, J. Warner, D. Starodub, J. C.H. Spence, and R. B. Doak. Gas dynamic virtual nozzle for generation of microscopic droplet streams. *J. Phys. D: Appl. Phys.*, 41, 2008.

[93] J. Schulz, J. Bielecki, R. B. Doak, K. Dörner, R. Graceffa, R. L. Shoeman, M. Sikorski, P. Thute, D. Westphal, and A. P. Mancusoa. A versatile liquid-jet setup for the european XFEL. *J. Synchrotron Radiat.*, 26: 339–345, 2019.

[94] L. Rayleigh. On the capillary phenomena of jets. *Proc. R. Soc. London*, 29:71–97, 1879.

[95] G. F. Taylor. Formation of thin flat sheets of water. *Proc. R. Soc. London, Ser. A, Math. Phys. Sci.*, 259(1296):1–17, 1960.

[96] Y.-B. Shen and D. Poulikakos. Thickness variation of a liquid sheet formed by two impinging jets using holographic interferometry. *J. Fluids Eng.*, 120(3):482–487, 1998.

[97] D. J. Hoffman, T. B. Van Driel, T. Kroll, C. J. Crissman, E. S. Ryland, K. J. Nelson, A. A. Cordones, J. D. Koralek, and D. P. DePonte. Microfluidic liquid sheets as large-area targets for high repetition XFELs. *Front. Mol. Biosci.*, 9:1048932, 2022.

[98] U. Weierstall. Liquid sample delivery techniques for serial femtosecond crystallography. *Philos. Trans. R. Soc. Lond. B Biol. Sci.*, 369(1647): 20130337, 2014.

[99] Y. Marcus. Surface tension of aqueous electrolytes and ions. *J. Chem. Eng. Data*, 55:3641–3644, 2010.

[100] R. R. T Marinho, M.-M. Walz, V. Ekholm, G. Öhrwall, O. Björneholm, and A. N. de Brito. Ethanol solvation in water studied on a molecular scale by photoelectron spectroscopy. *J. Phys. Chem. B*, 121(33):7916–7923, 2017.

[101] F Eschen, M Heyerhoff, H Morgner, and J Vogt. The concentration-depth profile at the surface of a solution of tetrabutylammonium iodide in formamide, based on angle-resolved photoelectron spectroscopy. *J. Phys.: Condes. Matter*, 7(10):1961, 1995.

[102] S. Mosallanejad, I. Oluwoye, A. Mohammednoor, J. Gore, and B. Z. Dlugogorski. Interfacial and bulk properties of concentrated solutions of ammonium nitrate. *Phys. Chem. Chem. Phys.*, 22:27698, 2020.

Printed by Media-Tryck, Lund 2024 NORDIC SWAN ECOLABEL 3041 0903

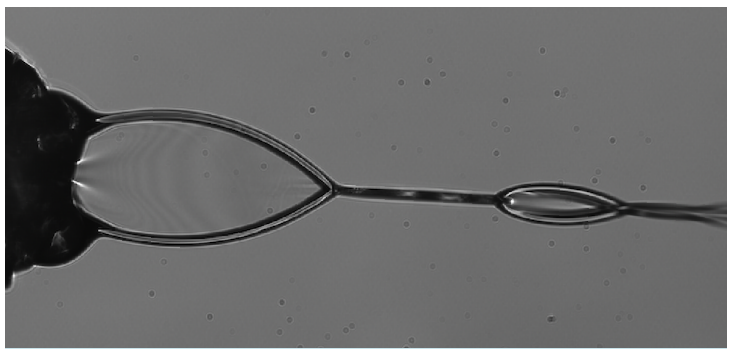

Faculty of Science
Department of Physics
ISBN: 978-91-8104-203-0